CEBAF Program Advisory Committee Eight Cover Sheet

This proposal must be received by close of business on Thursday, April 14, 1994 at:

CEBAF
User Liaison Office, Mail Stop 12 B
12000 Jefferson Avenue
Newport News, VA 23606

Proposal Title

In-plane Separations and High Momentum Structure in d(e,e'p)n

Contact Person

Name: Paul Ulmer
Institution: Old Dominion University
Address: Department of Physics
Address:
City, State ZIP/Country: Norfolk, VA 23529
Phone: (804) 683-5851 **FAX:** (804) 683-5809
E-Mail → Internet: ULMER @ CEBAF. GOV

Experimental Hall:	HALL A
Total Days Requested for Approval:	29
Minimum and Maximum Beam Energies (GeV):	0.4 - 4.0
Minimum and Maximum Beam Currents (μAmps):	30 - 50

CEBAF Use Only

Receipt Date: 11/14/94 PR 94-004

By: [illegible]

HAZARD IDENTIFICATION CHECKLIST

CEBAF Experiment: _____ Date: April 14, 1994

Check all items for which there is an anticipated need—do not check items that are part of the CEBAF standard experiment (HRSE, HRSH, CLAS, HMS, SOS in standard configurations).

Cryogenics ____ beamline magnets ____ analysis magnets ✓ target ____ drift chambers ____ other	**Electrical Equipment** ____ cryo/electrical devices ____ capacitor banks ____ high voltage ____ exposed equipment	**Radioactive/Hazardous Materials** List any radioactive or hazadorous/ toxic materials planned for use: _____ _____
Pressure Vessels ____ inside diameter ____ operating pressure ____ window material ____ window thickness	**Flammable Gas or Liquids** (incl. target) type: LH_2 / LD_2 flow rate: _____ capacity: _____	**Other Target Materials** ___ Beryllium (Be) ___ Lithium (Li) ___ Mercury (Hg) ___ Lead (Pb) ___ Tungsten (W) ___ Uranium (U) ___ Other (list below) _____ _____
Vacuum Vessels ____ inside diameter ____ operating pressure ____ window material ____ window thickness	**Radioactive Sources** ____ permanent installation ____ temporary use type: _____ strength: _____	**Large Mech. Structure/System** ____ lifting devices ____ motion controllers ____ scaffolding or elevated platforms ____ other
Lasers type: _____ wattage: _____ class: _____ **Installation** ____ permanent ____ temporary **Use** ____ calibration ____ alignment	**Hazardous Materials** ___ cyanide plating materials ___ scintillation oil (from) ___ PCBs ___ methane ___ TMAE ___ TEA ___ photographic developers ___ other (list below) _____ _____ _____	**Notes:** _____ _____ _____ _____ _____ _____

In-plane Separations and High Momentum Structure in d(e,e′p)n

C.E. Hyde-Wright, A. Klein, S. Kuhn, B. Raue, P.E. Ulmer (spokesman) and L. Weinstein
Old Dominion University, Norfolk, VA

M. Epstein
California State University at Los Angeles, Los Angeles, CA

J.M. Finn
The College of William and Mary, Williamsburg, VA

R. Ent, J. LeRose, R. Michaels, J. Mitchell and A. Saha
Continuous Electron Beam Accelerator Facility, Newport News, VA

Z. Papandreou
George Washington University, Washington, DC

R. Madey
Hampton University, Hampton, VA

B. Anderson, R. Madey and G. Petratos
Kent State University, Kent, OH

W. Bertozzi and S. Gilad
Massachusetts Institute of Technology, Cambridge, MA

V. Punjabi
Norfolk State University, Norfolk, VA

R. Gilman and C. Glashausser
Rutgers University, Piscataway, NJ

C.C. Chang and P. Markowitz
The University of Maryland, College Park, MD

J. Calarco
The University of New Hampshire, Durham, NH

G. Huber and G. Lolos
The University of Regina, Regina, SK

R.W. Lourie
The University of Virginia, Charlottesville, VA

and

The Hall A Collaboration

Abstract

This experiment will study the fundamental nucleus, ^{2}H. Using the capabilities of CEBAF we plan to considerably extend the present knowledge of the basic d(e,e′p)n reaction by studying the momentum distribution at higher momentum transfers and by undertaking separations of the R_L, R_T and R_{LT} response functions. The experiment consists of three cuts in the kinematic phase space all at quasifree ($x = 1$) kinematics. In the first cut the Q^2 dependence of the reaction will be examined by performing longitudinal/transverse (L/T) separations for protons emitted along $\vec{q}$ at Q^2=0.23, 0.81, 2.14 and 3.41 GeV^2/c^2 for $p_r = 0$. The second cut involves detecting protons away from the direction of $\vec{q}$ to determine the angular distribution of emerging protons for recoil momenta up to 0.5 GeV/c at a 3-momentum transfer of 1.0 GeV/c. From in-plane measurements on either side of $\vec{q}$ plus a backward angle measurement the R_T, R_{LT} and $R_L + R_{TT}$ components will be determined. In the third cut the R_{LT} response function will be extracted at a higher value of $\vec{q}$ (1.9 GeV/c) for recoil momenta up to 0.3 GeV/c. These measurements should provide checks on the model dependence of the reaction. In addition, R_{LT} is expected to be sensitive to relativistic effects, especially at these large values of Q^2 ($|\vec{q}|/m_N > 1$ where m_N is the nucleon mass), and so should provide a check on the validity of relativisitic treatments of the reaction. We believe that the proposed experiment will form an experimental basis for the study and interpretation of more exotic components of the reaction mechanism of this fundamental nuclear system.

This experiment is based on two previously submitted CEBAF Hall A proposals: PR-89-026 and PR-93-041

Status of Previous Proposals: Deferred

Date	Description	Beam Hours	Energies	Max. Luminosity
Apr. 14, 1994	^{2}H(e,e′p)n	700	0.4–4.0 GeV	1.5×10^{38}cm^{-2}sec^{-1}

CONTENTS

1. Response to PAC 6 Comments

This proposal was submitted to two previous CEBAF Program Advisory Committees: PAC4 and PAC6. In both cases the committee was concerned about the accuracy requirements of the experiment and recommended deferral of the proposal. At issue were target density fluctuations, luminosity monitoring and absolute measurement of the centroid beam energy. This section addresses each of these concerns.

1.1 Target Density Fluctuations

The report of PAC6 reads: "... some concern was felt about ... the stability of the target density at high beam current." There are several points which need to be made clear here.

i.) In fact, this proposal specifies using a fairly low beam current in order to keep density fluctuations to a minimum. The Hall A LD_2 cryotarget is being designed to provide cooling power of order 1000 Watts. For the maximum beam current assumed in the proposal (50 μA) the power dissipation in the target is 290 Watts, well below the design value.

ii.) It should be emphasized that the entire experiment (with the exception of one kinematic point) will be performed at the same beam current. An overall error in the assumed target density does not get magnified in extracting the response functions from the measured cross sections. Therefore, accurate knowledge of the target density is not required; rather the **time-averaged** target density should remain the same for the different kinematic points (each of which employs the same beam current). This requirement is much less difficult to guarantee.

iii.) As the L/T measurements require only 56 hours of beam time to complete (which is significantly less than the overhead of changing targets between LH_2 and LD_2) one could consider running at even lower luminosities without impacting significantly on the overall beam time requirement.

iv.) The angular distribution studies (which require the bulk of the beam time) will be performed at a fixed electron kinematics. Thus, the electron single-arm trigger rate will provide a relative luminosity monitor for each kinematic point.

v.) Finally, one can perform target density calibration measurements at low beam current (or as a function of beam current) for comparison with measurements taken at the higher beam currents employed in the experiment. For example, hydrogen elastic scattering could be used, although any measurement will serve to check the relative normalization of the target density.

The local heating effects can be quantified under certain assumptions. The local temperture rise caused by beam energy loss is:

$$\Delta T = \frac{I\frac{dE}{dx}}{x_b c_p v_s q_e}$$

where I is the beam current, dE/dx is the energy loss per electron in the target material per gm/cm^2, x_b is the horizontal extent of the beam spot, c_p is the specific heat of the target material, v_s is the flow velocity of the target fluid and q_e is the electron charge. This can be rewritten:

$$\Delta T\,[\mathrm{K}] = \frac{I\,[\mu\mathrm{A}]\ \frac{dE}{dx}\,[\mathrm{MeV}\cdot\mathrm{cm}^2/\mathrm{g}]}{x_b\,[\mathrm{cm}]\ c_p\,[\mathrm{J}/(\mathrm{g}\cdot\mathrm{K})]\ v_s\,[\mathrm{cm/s}]}$$

Evaluating this at the nominal operating parameters of the Hall A liquid deuterium target (T=20K, p=4 atm., c_p=6 J/(g·K), v_s=10^3 cm/s) for the conditions of the experiment (x_b=0.01 cm, I=50μA) and for dE/dx=2.4 MeV·cm^2/g gives ΔT=2.0K. Thus, with no rastering or defocussing of the beam, the temperture rise is 2.0K. However, target rastering will be available. If the raster sweeps over a distance a at frequency f, then the raster velocity is $2af$. If the vertical and horizontal extents of the beam spot are the same and if the rastering speed dominates over the flow velocity then the above temperture rise should be reduced by a factor of $v_s/(2af)$. Using the Hall A raster design goals of f=20 KHz and a=2 mm ($\pm$1 mm) gives a reduction factor of 1/8 (raster speed eight times higher than flow speed). The high flow velocities of the Hall A target insure that each successive sweep of the beam sees fresh target material. With this reduction factor of 1/8, the temperture rise is 0.25K. The Hall A cryotarget is subcooled by 1–2 K, so that this temperature rise should not cause any local boiling. Further, this temperture difference results in less than 0.5% density change of the liquid. In addition, at constant luminosity, this density change is the same for each kinematics therefore minimizing the errors in the extracted response functions.

1.2 Luminosity Monitoring

Here, there are two separate requirements: one for the absolute (overall) uncertainty in the luminosity for all kinematic points involved in a given separation measurement and one for the relative uncertainty from point to point.

i.) **Relative Luminosity:** For the angular distribution measurement, the electron spectrometer is fixed and so provides a relative luminosity monitor. Further, since the entire experiment will be performed with a fixed luminosity, the relative uncertainty from point to point is minimized. For the L/T separation measurements, the statistics acquired at low recoil momentum will be adequate to provide 1% measurements of the relative luminosity in each of several time bins for each measurement. This will serve as a check on the stability of the system.

ii.) **Absolute Luminosity:** As stated above, the proposed experiment is less sensitive to an overall uncertainty than to relative uncertainties. Thus, although the relative luminosity must be determined to a fraction of a percent, the absolute luminosity need only be known to several percent.

The schemes which have so far been considered for beam current measurement are the Parametric DC Current Transformer (PCT)[1] and stripline and cavity monitors. Preliminary tests of the PCT monitors indicate their resolution is adequate for relative current measurement at the fraction of a microamp level. This proposal would employ a 50μA beam current implying a relative measurement at the 1% level. The monitors would need to be calibrated periodically against an absolute standard (such as a wire fed by a calibrated current source). The stripline and cavity monitors are also expected to allow relative current measurement at 1% or better but would have to be calibrated against an absolute standard in order to provide an absolute measurement of the current.

Again, it is emphasized that the requirements of this experiment are not too demanding in terms of the absolute current measurement; a several percent measurement is adequate since an overall scale error does not get magnified in performing response function separations. Much of the Hall A physics program will also require current measurement at this level. As far as the relative measurement is concerned, the requirement is more stringent but also easier to guarantee.

1.3 Absolute Measurement of the Beam Centroid Energy

Substantial progress has been made with respect to techniques for beam centroid energy measurement. In September 1993 there was a series of meetings at CEBAF devoted to evaluating proposed methods for high accuracy beam energy measurements. These techniques are summarized and evaluated in CEBAF internal reports which are attached to this proposal.[2][3]

One of the most promising methods would employ photon endpoint energy measurements in Compton scattering. This method is non-destructive and is also free of the technical difficulties inherent in many of the magnetic measurement schemes where accurate field integral measurements are required.

Other techniques being pursued include p(e,e′p) elastic scattering using a dedicated (non-magnetic) high resolution silicon strip detector array as well as measurement of the bend angle in the arc beamline leading into Hall A. Both of these methods seem capable of measuring the absolute centroid energy at the few 10^{-4} level and possibly at the 10^{-4} level. Further, the arc measurement will continuously monitor relative changes in the beam energy at the 10^{-4} level.

Design and construction of the energy measurement systems are being undertaken by a French/CEBAF collaboration. The *ep* elastic scattering system is already being prototyped by a group at Clermont-Ferrand. Another group at Saclay will undertake either the arc

beamline or Compton scattering system; the decision will be taken this Summer. Further, the Compton technique is being considered for Hall C and various feasibility studies are planned for this year.

2. Introduction

2.1 Motivation for Studies of the Deuteron

This experiment will study the fundamental nucleus, ^{2}H. The deuteron, as the only bound two-nucleon system represents the simplest manifestation of the nuclear force. It therefore provides a benchmark in nuclear physics for one cannot hope to understand complex nuclei without first understanding the deuteron. Although the deuteron is the simplest nuclear system it is far from being well understood. Up to now every measurement of a new observable has presented us with a puzzle.

A study of the deuteron can reveal different aspects of the nuclear force depending upon the choice of reaction and kinematics. For example, backward angle deuteron electro-disintegration at threshold at high momentum transfers provides some of the most striking evidence to date of the existence of Meson Exchange Currents (MECs) in nuclei.[4] Studies of the tensor force as revealed by the deuteron quadrupole form factor through measurements of the tensor analyzing power, T_{20}, have been carried out for a variety of reactions and at various facilities and continues to be a topic of considerable interest (see [5] for example). Through measurements of elastic scattering at high momentum transfers and quasielastic breakup at large recoil momenta one is sensitive to the short range part of the nucleon–nucleon (NN) interaction. By studying the short distance structure of the deuteron wavefunction one may determine whether or to what extent the description of nuclei in terms of nucleon/meson degrees of freedom must be supplemented by inclusion of explicit quark effects. Such questions are of fundamental importance to nuclear physics.

Although the deuteron is a loosely bound system its high momentum structure (*i.e.* at large recoil momentum) is strikingly similar to that of more complex nuclei. This is revealed by a comparison of Saclay data on ^{3}He(e,e$'$p)np and d(e,e$'$p)n at high recoil momentum (see Figure 1).[6] Thus, measurement of high momentum components of the deuteron wave function can guide our understanding of the correlation structure of complex nuclei. Beyond 0.3 GeV/c recoil momentum one is primarily sensitive to the D-state component in the wave function. A precise measurement in this range would provide important constraints for nucleon-nucleon potentials. It should be emphasized however, that the momentum distribution is not an observable and can only be extracted in the context of a model. For example, final state interactions can significantly alter the momentum of the detected nucleon and therefore the inferred initial momentum. Studies of the deuteron will

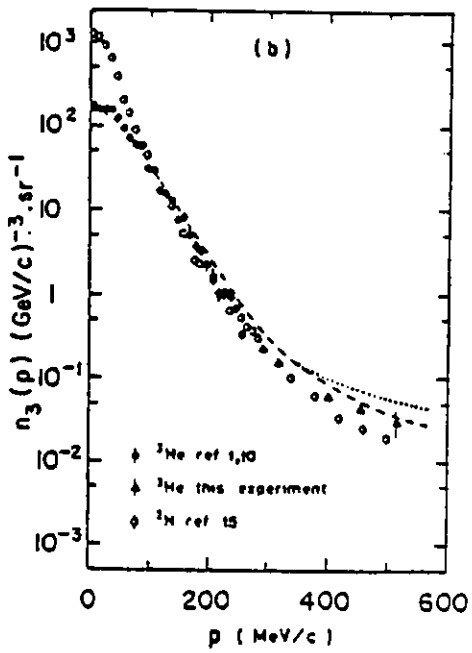

Figure 1. *Proton momentum distributions from the $^3He(e,e'p)np$ reaction. Also shown is the distribution from the electrodisintegration of ^2H.*

also help to pin down these effects (see below) so that more quantitative statements about the deuteron wave function can be made.

The deuteron's relative simplicity makes it the natural starting point for investigation of the nature of the nuclear electromagnetic current. The applicability of reaction models for complex nuclei can be gauged by the success of these models in reproducing scattering observables on the deuteron; our understanding of the deuteron is therefore critical to interpreting inclusive (e,e′) and coincidence (e,e′x) measurements for any nucleus.

Separations of electron scattering cross sections into longitudinal and transverse components provide further constraints on reaction models. For example, the transverse response function is generally more sensitive to MEC effects whereas the longitudinal response is, to first order, a measure of the one-body charge distribution. Failure of the Coulomb Sum Rule to describe the integrated longitudinal response for nuclei has aroused much controversy (see [7] for example). It is crucial to understand the longitudinal response first in the simplest nucleus, the deuteron.

Coincidence d(e,e′p)n reactions are particularly well suited to NN interaction studies. Below pion threshold, the final state is completely specified. For example, Fabian and Arenhövel have performed a nonrelativistic treatment of deuteron electrodistintegration in (e,e′p) in which they examined the importance of interaction effects (MECs and Isobar Configurations (ICs)) over the kinematical phase space below pion threshold.[8] Off the quasielastic peak they predict large changes in the transverse response due to the presense of these interaction effects. In particular, at low (high) momentum transfers and high (low) np relative energies, they expect large modifications from ICs (MECs). Therefore, by performing systematic studies over a broad kinematical range, the role played by various

interaction effects can be quantified. Further, at large values of Q^2 relativistic effects should be important. In fact, data at relatively low Q^2 from NIKHEF already indicate the need for a relativistic treatment in order to properly describe the R_{LT} response function.[9][10]

The deuteron is a valuable tool not only for what it can tell us about the nuclear force but also as a source of neutrons. Lacking pure neutron targets, the deuteron with its relatively loose binding is often chosen for studies of the structure of the neutron. Measurements of elastic[11] and quasielastic[12] electron scattering from deuterium have been used extensively in order to extract the long sought after and poorly known neutron electric form factor, G_{En}. There is also considerable interest in $d(\vec{e},e'\vec{n})p$ polarization transfer measurements since various calculations predict that at small recoil momentum the observable of interest is sensitive to G_{En}[13] but relatively insensitive to NN interaction effects and to the deuteron wavefunction[14]. Such an experiment has been carried out recently at the Bates Linear Accelerator Center.[15] The full potential of such measurements will be realized with the advent of high duty factor electron accelerators (see [16] for example). Understanding the deuteron is also vitally important for measurements employing deuterium targets to determine the spin structure function of the neutron.

All of the above neutron studies rely on the assumption that nuclear corrections for the deuteron are either small or well understood. It is therefore vitally important to these measurements that this assumption be thoroughly tested. In particular, since the neutron form factor studies via $d(\vec{e},e'\vec{n})p$ will be performed at small recoil momentum, p_r, where the aforementioned theoretical calculations predict minimal influence from interaction effects, it is crucial that the deuteron be understood in this kinematical region. In light of the fact that data on d(e,e′p)n from Saclay[17] are at variance with respect to theory near $p_r = 0$ and with respect to more recent data from NIKHEF[18], further measurements of this reaction should prove invaluable. In addition, approved experiments at Bates and CEBAF on $d(\vec{e},e'\vec{p})n$[19] will exploit the known proton form factors to test the model assumptions for the $d(\vec{e},e'\vec{n})p$ experiments.

If one wishes to describe nuclei in terms of nucleon/meson degrees of freedom, a natural question arises as to whether nucleon properties become modified inside a nucleus. It is, of course, arguable whether "medium modified nucleons" are the appropriate degrees of freedom with which to describe nuclei under certain circumstances and at the very least their characterization only makes sense in the context of a reaction model. Nonetheless, this topic has received considerable attention, both theoretical and experimental. One of the ways in which medium effects can manifest themselves is via so-called "off-shell" effects. For example, the current operator for an initially bound nucleon is ambiguous.[20] Also, there are dynamical effects in which the nucleon form factors and spinors are modified compared to their free-space values. Extraction of the bound nucleon form factors requires detailed understanding of the reaction model. The best candidate for such a study is the d(e,e′p)n reaction. Although the deuteron is loosely bound, measurements at high recoil momenta can be sensitive to off-shell effects and its relative simplicity makes it the best hope for controlling the other aspects of the problem. In addition, due to the

small mass of the recoil as compared to that for (e,e′p) reactions on heavier systems, there is a kinematical enhancement with respect to the current operator's sensitivity to the degree of "off-shellness". Although such a study is not the focus of the proposed d(e,e′p)n experiment, the expected sensitivities of this reaction to off-shell effects are summarized in the Appendix.

2.2 Formalism

The kinematics for (e,e′p) are depicted in Figure 2. In the One Photon Exchange Approximation (OPEA) the unpolarized (e,e′p) cross section can be written in terms of four independent nuclear structure functions[21]:

$$\frac{d^4\sigma}{d\omega d\Omega_e dT_p d\Omega_p} = \sigma_M \left[v_L R_L + v_T R_T + v_{LT} R_{LT} \cos\phi_x + v_{TT} R_{TT} \cos 2\phi_x \right].$$

The more general case, including beam and recoil polarization has been worked out in detail.[22] The response functions depend on $\vec{q}$, ω, θ_{pq} (the proton angle with respect to $\vec{q}$) and ϵ_m (the missing mass). (For a discrete final state (*i.e.* fixed ϵ_m) the response functions are determined by only three quantities.) ϕ_x is the angle between the electron scattering plane and the plane containing $\vec{q}$ and the detected proton. The v's are known kinematic factors weighting the various virtual photon polarization states and σ_M is the Mott cross section. The response functions, R, represent various products of components of the nuclear electromagnetic current. By varying the kinematics so as to keep the response functions fixed, each may be separately determined isolating various components of the nuclear current. In-plane measurements are capable of separating the R_T and R_{LT} term from a linear combination of the R_L and R_{TT} terms. At quasifree kinematics the R_{TT} term tends to be small. For the special case $\theta_{pq} = 0$ (parallel kinematics) only the longitudinal, R_L, and transverse, R_T, response functions survive.

2.3 Overview of Existing Data

Most of the early coincidence work on deuterium was obtained via (p,2p) rather than (e,e′p) reactions, since the scattering cross sections are comparatively large. The most precise (p,2p) measurement differs from (e,e′p) data by more completely satisfying the sum-rule.[23] Earlier (p,2p) data at high recoil momentum exhibited a large enhancement (up to a factor of 10) compared to Impulse Approximation (IA) calculations.[24] However, in a more recent experiment, most of this discrepancy was resolved by comparing the newer data with a more realistic calculation including the effects of rescattering.[25] Compared to (p,2p) reactions, the reaction dynamics in (e,e′p) are relatively simple since one does not have to consider large initial state distortions arising from the probe. The advent of high intensity and moderate duty factor electron accelerators has made such experiments possible and CEBAF will allow very precise measurements over a previously unobtainable kinematical range.

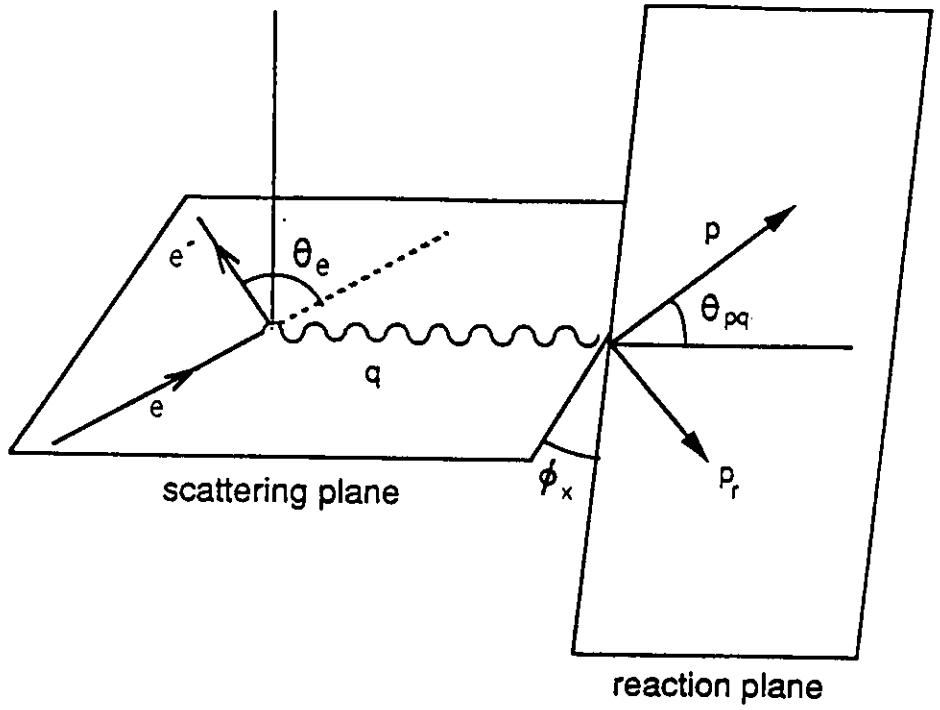

Figure 2. *Kinematics for (e,e'p). Here e (e') is the energy of the incident (scattered) electron, θ_e is the electron scattering angle, p is the momentum of the detected proton, θ_{pq} is the angle of the detected proton with respect to $\vec{q}$, p_r is the recoil momentum and ϕ_x is the angle between the reaction and scattering planes.*

Present knowledge of d(e,e'p)n reactions is fragmentary. Due to the low energies and duty factors of existing accelerators, only a few measurements at relatively low Q^2 and with modest statistical precision have been performed. The most extensive study to date is a measurement of the momentum distribution by the Saclay group in the region $0 \leq p_r \leq 0.175$ GeV/c (at $\vec{q} = 0.45$ GeV/c and $x = 0.97$) and in the region $0.155 \leq p_r \leq 0.335$ GeV/c (at $\vec{q} = 0.35$ GeV/c and $x = 0.36$).[17] The second measurement was performed at lower $\vec{q}$ in order to maximize the counting rate and was also off the quasielastic peak. The data along with a calculation employing the Paris nucleon-nucleon potential [26] and a calculation employing a relativistic one boson-exchange description[27] are shown in Figure 3. (Also shown is a parametrization due to Krautschneider[28] which is the one used for counting rate estimates in this proposal.) It is clear from the figure that the data stops where the models begin to deviate significantly. Even more striking is the large discrepancy ($\sim$ 30%) between the models and the data near $p_r = 0$. One cannot confidently interpret d(e,e'n) data in terms of neutron form factors until the origin of this anomaly is understood. In addition to the above data near the quasielastic peak, Turck-Chieze *et al.* have studied the contribution of Δ mechanisms at high recoil momentum (0.3–0.5 GeV/c) for $\vec{q} = 0.28$ GeV/c and $x = 0.10$.[29]

So far, only a few measurements involving separation of the electromagnetic response functions in d(e,e'p) have been performed. The first such measurement was a very low energy experiment performed at Tohoku University.[30] The only other published separations were performed recently at NIKHEF where the longitudinal and transverse response

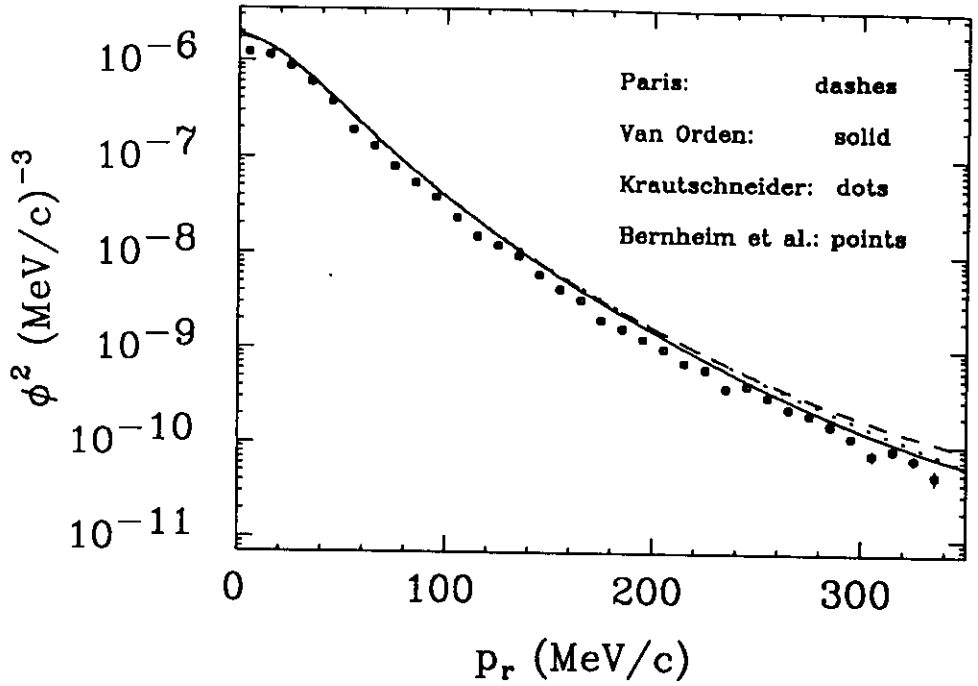

Figure 3. *Bernheim d(e,e'p)n data from Saclay along with various calculations described in the text.*

functions at $\vec{q} \leq 0.50$ GeV/c and $p_r \leq 0.11$ GeV/c[31] and the longitudinal-transverse interference response function at $\vec{q} = 0.46$ GeV/c and $p_r \leq 0.18$ GeV/c[9] were measured. Although the ratio of the transverse to longitudinal response functions agrees well with both relativistic and nonrelativistic calculations the calculations underestimate both response functions in an absolute sense. For the LT interference response function the authors indicate the need for a relativistic calculation even at the relatively low momentum transfer of the experiment. This can be seen from Figure 4 where the LT response function data are shown along with relativistic and nonrelativistic calculations. Measurements at higher momentum transfers and with smaller error bars would be very useful in determining the validity of the relativisitic treatment. (Although a measurement of the R_{LT} interference response function at relatively high Q^2 ($Q^2 = 1.2$ GeV^2/c^2) was recently carried out at SLAC, the data only extends to recoil momenta of 0.17 GeV/c with fairly large uncertainties.[32]) Finally, a program of measurements of the d(e,e'p)n response functions at relatively low $\vec{q}$ is underway at Bates. Initial measurements of the in-plane response functions have been made and will be supplemented by measurements of protons out of the scattering plane to extract the transverse-transverse interference response function.

2.4 Experiment Proposal Overview

This proposal differs from previous (e,e'p) measurements by exploiting the dynamical range and high duty factor anticipated at CEBAF to explore the reaction over a large range of $\vec{q}$ and to high recoil momentum. This initial study proposes to examine the unpolarized response functions in the region of the quasielastic peak ($x = 1$). Both the $\vec{q}$ dependence (at $p_r = 0$) and the recoil momentum dependence (at $\vec{q} = 1.0$ GeV/c and at $\vec{q} = 1.9$ GeV/c) will be explored.

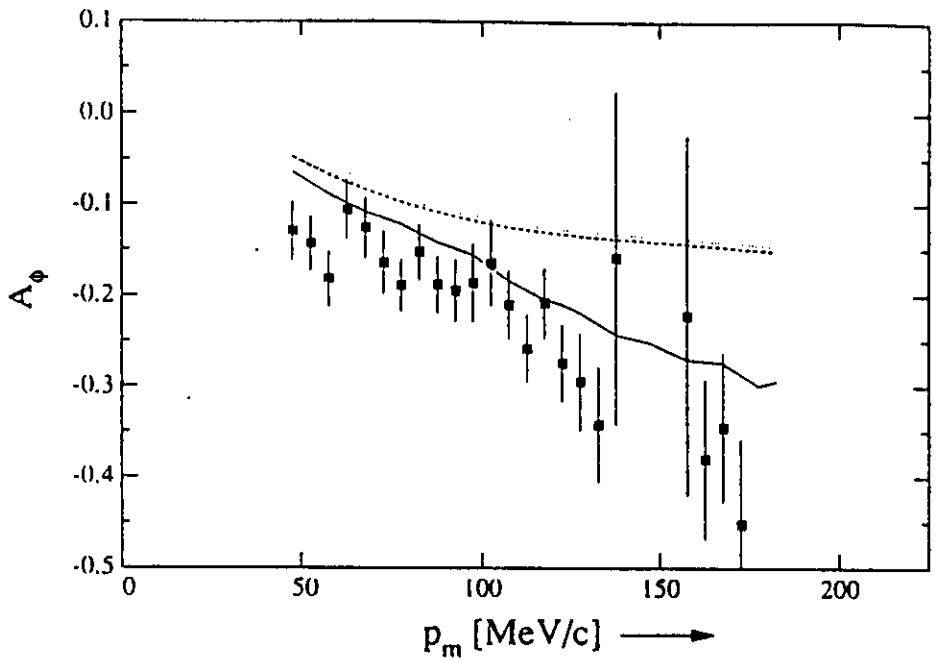

Figure 4. ***LT interference response function measured at NIKHEF along with various calculations. The solid curve is for the relativistic treatment. The other curves are nonrelativistic calculations and are seen to deviate from the data significantly.***

Three sets of measurements of d(e,e′p)n are proposed, all at quasifree kinematics ($x = 1$):

i.) An L/T separation for protons emitted along $\vec{q}$ at Q^2 of 0.23, 0.81, 2.14 and 3.41 GeV^2/c^2. This measurement will be performed at $p_r = 0$, although the spectrometer acceptances result in recoil momenta up to 0.25 GeV/c being sampled for the forward angle kinematics at all but the lowest Q^2 point. The lowest Q^2 point is included to match on to measurements taken at existing facilities and requires very little beam time.

ii.) A measurement of the angular distribution of protons up to 0.5 GeV/c recoil for $\vec{q} = 1.0$ GeV/c. These measurements will be made at constant momentum transfer and invariant mass thereby fixing the relative momentum in the center of mass of the recoiling proton-neutron pair. For a given recoil momentum the virtual photon longitudinal polarization is varied by making forward and backward angle measurements allowing a separation of R_T and the sum of R_L and R_{TT}. The LT interference response function is separated by detecting protons on either side of $\vec{q}$ at the forward angle.

iii.) A measurement of the angular distribution of protons up to 0.3 GeV/c recoil for $\vec{q} = 1.9$ GeV/c. The same measurement philosophy is employed here as in the previous angular distribution study, except due to count rate limitations the backward angle kinematics will be omitted. Measurements on both sides of $\vec{q}$ will be made to separate the R_{LT} response.

In general, the extraction of the momentum distribution can only be done in the context of some reaction model. Relative to a single-particle knockout model the effective momentum distribution can be sensitive to the choice of kinematics. For example, at high recoil momentum ($\sim$ 0.5 GeV/c) virtual Δ channels can affect the results by as much as a factor of two for some kinematics.[29] Therefore, follow-up measurements to study the systematics of the reaction process would be greatly desired.

The high energies afforded by CEBAF will make it possible to perform precise L/T separations at momentum transfers much larger than at existing facilities. In addition, the combination of high energy and duty factor will allow, for the first time, examination of very high recoil momenta while keeping the kinematics quasielastic. For much of the experiment, high resolution spectrometers are crucial since systematic errors in the cross section are magnified in determining the response functions. The longitudinal response function becomes especially difficult to determine accurately above momentum transfers of 2 GeV/c due to its small relative size. This experiment on the deuteron will include L/T separations up to the practical limit and will constitute an important test of reaction models.

It is clear that one must perform precise systematic studies of the d(e,e′p)n reaction in order to be able to disentangle features of the wave function and electromagnetic current. This proposal should therefore be viewed as one component in a much broader program of measurements. The quasielastic kinematics explored here should serve as a first calibration of the model for the deuteron. Additional non-quasielastic ($x \neq 1$) kinematics where interaction effects are expected to play a larger role will be subsequently explored. In addition it is envisioned that the complete program will include out-of-plane measurements and measurements of spin observables. (A separate proposal to study polarization transfer in d($\vec{e}$,e′$\vec{p}$)n in Hall A has been approved by the CEBAF PAC[19].)

2.5 Theoretical Calculations and Measurement Uncertainties

To indicate the quality of the anticipated data and the model sensitivity for the low Q^2 angular distribution measurement the coincidence cross section is plotted in Figure 5 for a kinematics close to that of the proposed experiment for two models of the NN interaction[26][27]. As indicated below, the current data stops at $p_r = 335$ MeV/c[17] although measurements at higher recoil momenta have been performed in the delta-resonance region[29]. The actual proposal samples up to $\sim$ 550 MeV/c recoil although one could push the measurement to 600 MeV/c as indicated for modest additional beam time but without separations. As can be seen from the figure, the model sensitivity in the region probed by this experiment is enormous and therefore this experiment should provide stringent constraints on NN interaction models.

Fabian and Arenhövel[8] have performed a nonrelativistic theoretical treatment of the (e,e′p) reaction for the case of the deuteron, including effects from Final State Interactions (FSI), Meson Exchange Currents (MEC) and Isobar Configurations (IC). A calculation

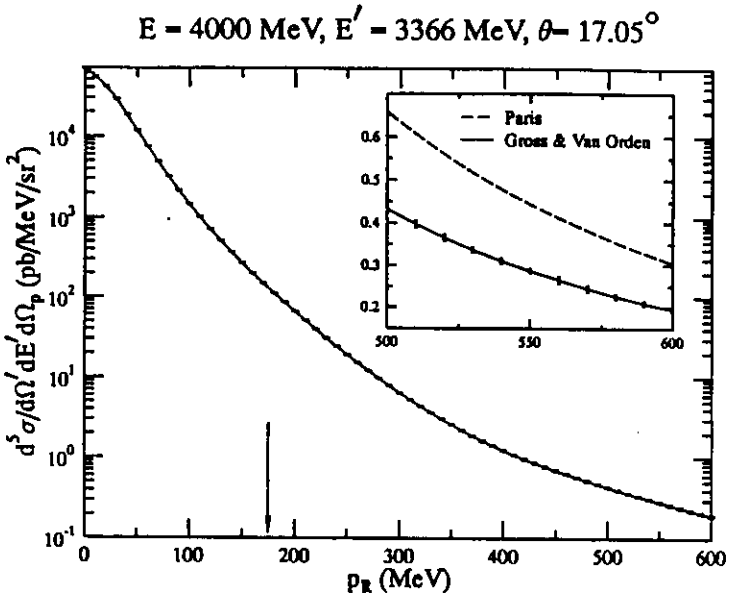

Figure 5. *Recoil momentum range and statistical error bars for a kinematics close to those of the proposal. The beam time estimate does not include the data from 550 to 600 MeV/c although it could be obtained with modest additional time for the forward angle kinematics.*

of the four unpolarized response functions for $\vec{q} \sim 1$ GeV/c and quasielastic kinematics ($x = 1$) is shown in Figure 6 versus θ_{cm} (the angle of the recoiling np pair relative to $\vec{q}$ in the center of mass) for the range of angles sampled in the proposed experiment.[33] The R_{TT} term which can only be separated via an out-of-plane measurement is quite small for small θ_{cm} but becomes comparable to R_L for larger θ_{cm}. In Figure 7, ratios of each of the separate ingredients in Arenhövel's model to his full calculation are shown for the combinations of response functions accessible to the measurement along with the projected uncertainties of the data. In order to be conservative, the error bars shown in the figure assume systematic uncertainties roughly three times larger than those which we hope to ultimately obtain using the Hall A high resolution spectrometers. The total systematic uncertainties in the cross sections are assumed to be 4.5% for the two forward electron angle kinematics and 1.5% for the backward kinematics and are also taken to be independent of θ_{cm} (these errors are thus three times larger than the peak values expected for the range of θ_{cm} covered - see the section on Analysis of Systematic Uncertainties). In addition, the errors shown include statistical uncertainties added in quadrature to the systematic uncertainties. Finally, the error bars without caps include an overall 5% additional systematic error on the response functions. This error reflects uncertainties which affect all cross sections equally (such as an uncertainty in the scale for the beam current measurement). Even though the total uncertainties shown are substantially larger than what we hope to achieve, the projected data exhibits considerable sensitivity to the ingredients of Arenhövel's model. For large θ_{cm}, all the response functions are quite sensitive to FSI effects and R_T is somewhat sensitive to interaction effects (MECs and ICs) as well. Although R_L is expected to be least sensitive to these interaction effects, measurements over a range of Q^2 should provide a starting point from which to calibrate deuteron models and may, for example, also shed

light on the Coulomb Sum Rule mystery alluded to earlier. In summary, by separating response functions one can sort out the various contributions to the reaction.

Although the above calculation is nonrelativistic, it serves as a guide for the experimental program at CEBAF. Additional calculations of the effects of MEC and FSI on the angular distribution and polarization of protons in d(e,e'p) have been undertaken by groups in the USSR and France.[34] Furthermore, fully relativistic calculations have been carried out by Hummel and Tjon[10] and are currently underway by Van Orden and Gross.[35] These theoretical groups have all expressed interest in performing calculations for deuterium at CEBAF kinematics.

To indicate the sensitivity to relativistic effects, a calculation of Tjon[36] is displayed in Figure 8 for the low Q^2 angular distribution kinematics. The data with anticipated error bars are shown on top of the relativistic calculation (solid curve). (Actually, the errors shown assume that all kinematical uncertainties are uncorrelated. This is therefore an overestimate of the error since the two measurements used to separate the LT interference response are at the same electron kinematics.) There is considerable sensitivity to relativistic effects here and this sensitivity is likely to grow with Q^2. Thus, this measurement along with the high Q^2 angular distribution measurement should prove valuable in verifying the validity of the relativistic treatment.

2.6 Summary of Goals for this Proposal

This experiment will provide detailed information on the d(e,e'p)n reaction at quasifree ($x = 1$) kinematics. Such studies will serve as a measure of our understanding of nuclei in general since any successful model must first correctly predict observables for this simplest system. The following summarizes the goals of the proposed experiment:

- We will undertake separations of the d(e,e'p)n longitudinal and transverse response functions near $p_r = 0$ over a large range of Q^2. One of the very important open questions here is the origin of the anomoly in the existing data[17] relative to theory near $p_r = 0$. It is important that this be understood if one is to reliably interpret existing and planned neutron form factor studies employing deuterium as the target. The size of the discrepancy ($\sim 30\%$) suggests that although much of this proposal requires high precision, some important issues can be resolved with modest precision. The Q^2 dependence of the longitudinal and transverse response functions can shed light on the mystery with respect to the Coulomb Sum Rule (R_L) and can quantify the importance of interaction effects (R_T mostly) at quasifree kinematics.

- We will measure the recoil momentum distribution in d(e,e'p)n at $\vec{q} = 1.0$ GeV/c over a wide range of recoil (up to $p_r = 0.5$ GeV/c) at quasifree kinematics. This measurement will be the first to sample high ($p_r > 0.3$ GeV/c) recoil at quasifree

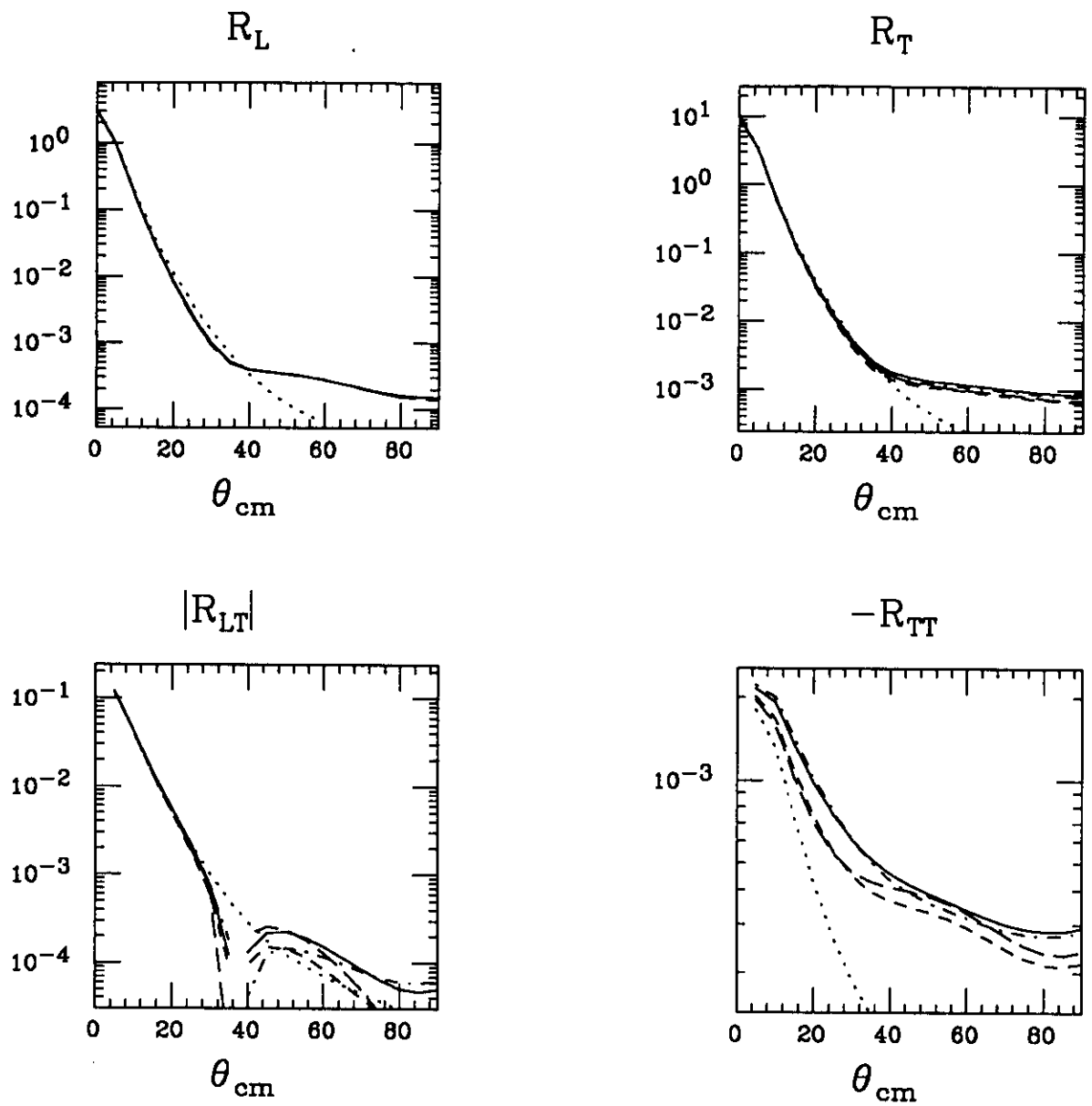

Figure 6. *The four unpolarized response functions as calculated by Arenhövel for $\vec{q} \sim 1$ GeV/c and quasielastic kinematics ($x = 1$). The curves for R_{LT} are negative below $\theta_{cm} = 35°$ and the PWBA R_{LT} curve is negative everywhere. Although the response functions have been calculated for θ_{cm} up to 180° they are only displayed over the range accessible to this experiment. The dotted curve is PWBA (Plane Wave Born Approximation; including the neutron exchange term), the short dashed curve includes FSI, the dot-dash curve is FSI+MEC, the long dashed curve is FSI+IC and the solid curve is the total result (FSI+MEC+IC).*

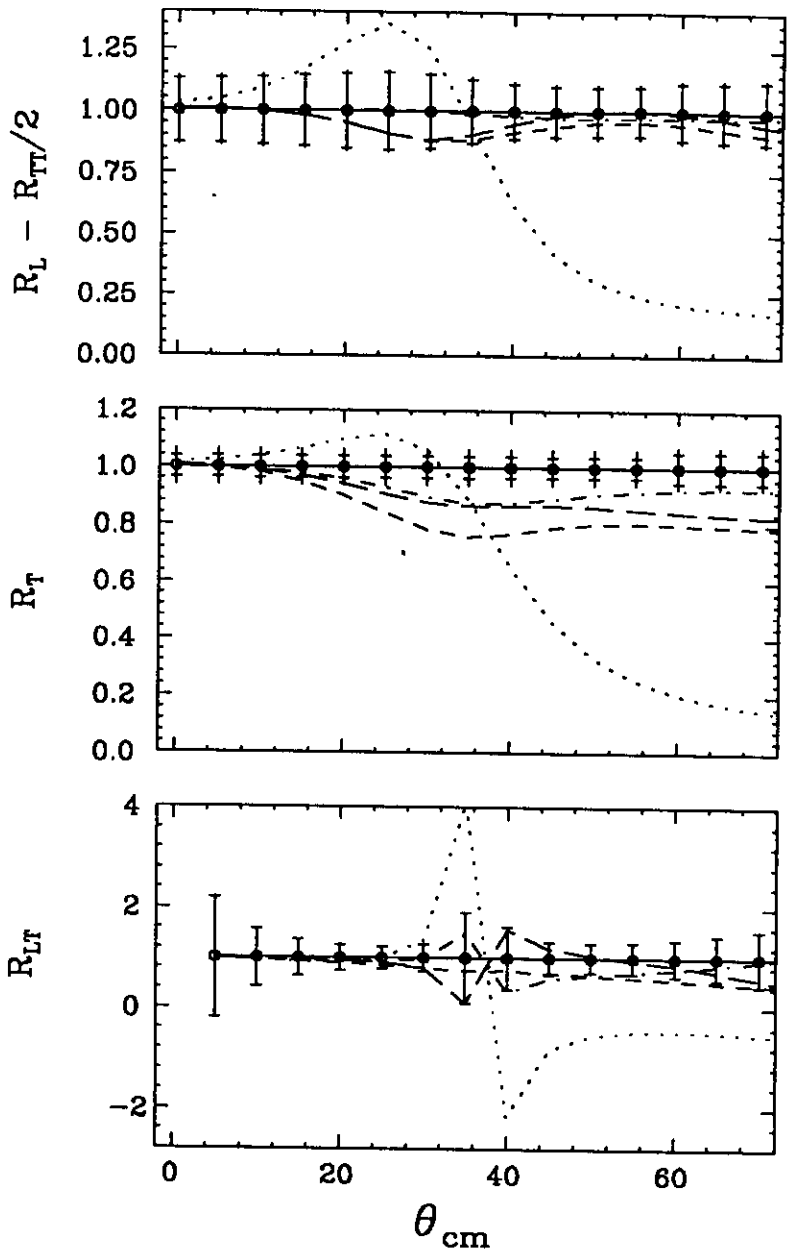

Figure 7. *Ratios of each of the separate ingredients in Arenhövel's model to his full calculation for the combinations of response functions accessible to the measurement along with the projected uncertainties (systematic and statistical) of the data. The curves are labeled as in the previous figure. In order to be conservative, the error bars shown in the figure assume systematic uncertainties roughly three times larger than those which we hope to ultimately obtain (see the text for details). Also, the error bars without caps include an additional 5% systematic uncertainty on the response functions (reflecting an uncertainty which affects all cross section measurements equally).*

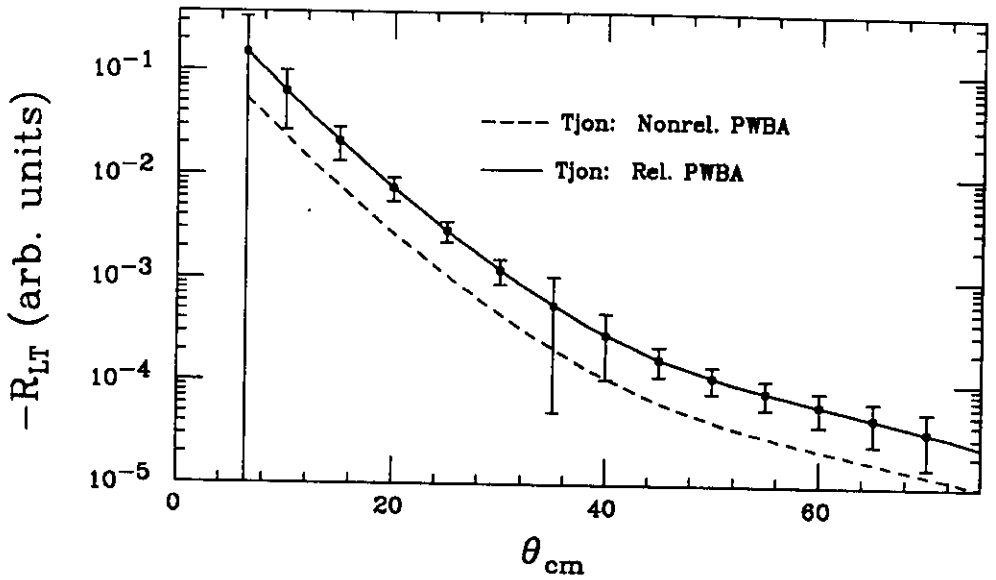

Figure 8. *The R_{LT} response function as calculated by Tjon for the low Q^2 angular distribution measurement. The solid curve is the relativistic calculation and the dashed curve is a nonrelativistic reduction. The projected uncertainties for the experiment are also displayed (see Figure 7 for details). These errors assume the kinematical uncertainties are all uncorrelated and are therefore an overestimate (see the text for details).*

kinematics and should help to pin down the short-range aspects of the nucleon-nucleon interaction. Measurements above $p_r = 0.3$ GeV/c will constrain the D-state component of the deuteron wavefunction thereby giving information on the NN tensor interaction.

- We will undertake separations of the response functions for the above recoil momentum dependence measurement. Such separations are crucial to understanding details of deuteron models. In particular, R_L is expected to be relatively insensitive to interaction effects and therefore serves as a benchmark for any model of the deuteron. R_T, R_{LT}, and especially R_{TT} are expected to be more sensitive to interaction effects. In addition, the R_{TT} response function can become appreciable compared to the other response functions for high recoil momenta, although its separation requires an out-of-plane measurement.

- We will also separate the R_{LT} response function at $\vec{q} = 1.9$ GeV/c for recoil momenta up to 0.3 GeV/c. At this large momentum transfer ($|\vec{q}|/m_N > 1$ where m_N is the nucleon mass) relativistic effects should be important. Therefore, this measurement combined with the lower Q^2 R_{LT} measurement will be valuable in verifying the validity of relativistic treatments of the reaction.

- Although the question of the off-shell character of bound nucleons can only be answered if one believes one has an understanding of the various interaction effects to be addressed by these measurements, the proposed experiment is expected to

exhibit sensitivity to off-shell effects. Their Q^2 dependence can be examined as a function of recoil momentum (related to the degree of "off-shellness") for the above parallel kinematic measurements (here the spectrometer acceptances allow examination of recoil momenta from 0 to 0.25 GeV/c at a single kinematic setting for the forward angle measurements) as well as for the angular distribution studies in perpendicular kinematics.

Only through systematic studies such as these can one hope to disentangle the features of the deuteron wavefunction and electromagnetic current. Even so, it is envisioned that this experiment respresents only a part of a larger program including measurements off the quasielastic peak ($x \neq 1$) as well as measurements of out-of-plane and polarization observables.

3. Details of the Experiment

3.1 Kinematics

In this section the kinematics for the L/T separation measurements as well as for the proton angular distribution measurements are discussed.

The L/T separation measurements are of fundamental importance in disentangling the various contributions to the reaction and require no special apparatus in addition to the two spectrometers (e.g. polarimeters or out-of-plane capability). Each measurement employs parallel kinematics (outgoing proton detected along $\vec{q}$, the three momentum-transfer) so that the interference response functions do not contribute. Although parallel kinematics cannot be maintained everywhere over a finite acceptance, the interference response functions average to zero in the case of a symmetric ϕ_x acceptance. In this case the cross section reduces to a sum of two terms:

$$\frac{d^4\sigma}{d\omega d\Omega_e dT_p d\Omega_p} = k\sigma_M \left[\frac{2Q^2}{\vec{q}^2}\epsilon R_L + R_T\right]$$

where k is a kinematical factor and ϵ is the longitudinal virtual photon polarization defined as

$$\epsilon = \left[1 + \frac{2\vec{q}^2}{Q^2}\tan^2(\theta_e/2)\right]^{-1}.$$

We examined four values of momentum transfer. (The smallest momentum transfer point ($Q^2 = 0.234$ GeV^2/c^2; $\vec{q} = 0.5$ GeV/c) is included to match on to measurements which can be performed at existing facilities.) The kinematics are given in Table 1A and are centered at recoil momentum, $p_r = 0$. (At the forward electron angles a recoil momentum range of 0–0.25 GeV/c is covered by the spectrometer coincidence acceptance for all but the lowest Q^2 point.) A maximum beam energy of 4 GeV was assumed although a larger beam energy would be advantageous for the higher Q^2 points since it would allow more forward electron angles and therefore larger virtual photon polarization lever arms. To minimize

energy changes we have selected our kinematics to use energies which are multiples of the maximum single-pass energy of 0.8 GeV. Ignoring the energy of the injector this gives a five-pass energy of 4 GeV. By doing this all the measurements can be made at a single machine energy of 4 GeV, except for the backward angle energy of 0.4 GeV at the lowest Q^2 point which can be reached with a five pass energy of 2 GeV. In arriving at these kinematics, minimum momenta of 0.27 GeV/c and minimum angles of 12.5° were assumed for both spectrometers. It is important that the spectrometers be able to reach small forward angles since small electron angles allow us to maximize the longitudinal polarization and cross sections while for backward electron angles the proton tends to be emitted in the forward direction.

Kin	Q^2 GeV^2/c^2	e GeV	ω GeV	T_p GeV	θ_e deg	θ_p deg	ϵ
IF	0.234	1.6	0.127	0.125	18.12	−66.40	0.948
IB		0.4			94.08	−32.98	0.289
IIF	0.811	4.0	0.435	0.433	13.69	−57.55	0.966
IIB		0.8			112.88	−19.64	0.151
IIIF	2.139	4.0	1.145	1.143	25.00	−40.51	0.863
IIIB		1.6			117.96	−12.50	0.101
IVF	3.408	4.0	1.823	1.821	36.46	−29.91	0.700
IVB		2.4			103.33	−12.50	0.137

Table 1A *Kinematics for the L/T Separation Measurements*

Next, we will explore the angular distribution of protons for recoil momenta up to 0.5 GeV/c at a momentum transfer of $\vec{q} = 1.0$ GeV/c. The invariant mass is held constant and the kinematics are quasifree ($x = 1$). By making measurements on either side of the $\vec{q}$ direction the R_{LT} interference response function can be isolated. Denoting the measured cross section by σ, we have:

$$\sigma_{LT} = [\sigma(\phi_x = 0) - \sigma(\phi_x = \pi)]/2.$$

In addition, the R_T response function can be separated by making an additional measurement at a backward electron angle. The R_L response function cannot be separated from the R_{TT} response function without an out-of-plane measurement so this experiment will measure a linear combination of these responses. The cross sections are calculated for eight kinematics centered at recoil momenta of 0, 0.05, 0.10, 0.15, 0.20, 0.30, 0.40 and 0.50 MeV/c. The actual measurements will be made by moving the spectrometer in a set of overlapping steps allowing a uniform measurement of the response functions as a function

of recoil momentum or angle. The $p_r = 0$ point is at the same kinematics as for the L/T separation (Kinematics IIF/IIB). The proton final momentum and angle are correlated for fixed electron kinematics and were varied to achieve the desired value of p_r. By keeping the relative energy in the center of mass of the recoiling np pair fixed, variations in the final-state interaction are minimized. Tables 1B and 1C summarize the kinematics.

Finally, the R_{LT} response function will be separated at $\vec{q} = 1.9$ GeV/c for recoil momenta up to 0.3 GeV/c and for $x = 1$. The $p_r = 0$ point is at the same kinematics as for the L/T separation (Kinematics IIIF). Here, only the forward electron angle measurements will be performed (one measurement on either side of $\vec{q}$ at each recoil momentum); the backward electron angle measurement will not be made due to count rate limitations. As in the lower Q^2 angular distribution measurement, the electron kinematics are fixed and only the proton momentum and angle are varied. Table 1D summarizes the kinematics.

$\vec{q}$ GeV/c	e MeV	ω MeV	θ_e deg	ϵ
1.0	4000.0	435.2	13.69	0.966
Kin	p_r MeV/c	T_p MeV	θ_p deg	θ_{cm} deg
0A/B	0	433.0	−57.55	0
50A/B	50	431.7	−54.68/−60.42	6.36
100A/B	100	427.7	−51.81/−63.29	12.72
150A/B	150	421.1	−48.93/−66.17	19.08
200A/B	200	412.0	−46.02/−69.08	25.49
300A/B	300	386.3	−40.13/−74.97	38.36
400A/B	400	351.4	−33.05/−81.05	51.47
500A/B	500	308.2	−27.69/−87.41	64.94

Table 1B *Kinematics for the low Q^2 proton angular distribution measurement at the forward electron angle. The final state np relative energy in the center of mass, E_{pn}^{cm}, is fixed at 206 MeV and the momentum transfer in the center of mass, $\vec{q}_{cm}$ is 901 MeV/c.*

3.2 Counting Rate and Background Estimates

Counting rates were based on the spectrometer acceptances given in Table 2 where $\theta_{V(H)}$ is the vertical (horizontal) spectrometer angular acceptance. All rates assume a

$\vec{q}$ GeV/c	e MeV	ω MeV	θ_e deg	ϵ
1.0	800.0	435.2	112.88	0.151
Kin	p_r MeV/c	T_p MeV	θ_p deg	θ_{cm} deg
0C	0	433.0	−19.64	0
50C	50	431.7	−22.51	6.36
100C	100	427.7	−25.38	12.72
150C	150	421.1	−28.62	19.08
200C	200	412.0	−31.17	25.49
300C	300	386.3	−37.06	38.36
400C	400	351.4	−43.14	51.47
500C	500	308.2	−49.50	64.94

Table 1C *Kinematics for the low Q^2 proton angular distribution measurement at the backward electron angle. The final state np relative energy in the center of mass, E_{pn}^{cm}, is fixed at 206 MeV and the momentum transfer in the center of mass, $\vec{q}_{cm}$ is 901 MeV/c.*

$\vec{q}$ GeV/c	e MeV	ω MeV	θ_e deg	ϵ
1.86	4000.0	1145	25.00	0.863
Kin	p_r MeV/c	T_p MeV	θ_p deg	θ_{cm} deg
0D/E	0	1143	−40.51	0
100D/E	100	1138	−37.43/−43.59	7.81
200D/E	200	1122	−34.34/−46.67	15.61
300D/E	300	1096	−31.26/−49.76	23.34

Table 1D *Kinematics for the high Q^2 proton angular distribution measurement. The final state np relative energy in the center of mass, E_{pn}^{cm}, is fixed at 504 MeV and the momentum transfer in the center of mass, $\vec{q}_{cm}$ is 1464 MeV/c.*

luminosity of 81 μA-g/cm^2 ($= 1.5 \times 10^{38}$ cm^{-2}sec^{-1}) unless indicated otherwise. This luminosity corresponds to 50 μA of beam on a 10 cm LD_2 target.

Acceptance averaged (e,e'p) cross sections were calculated in the Plane Wave Impulse Approximation (PWIA) using the computer program MCEEP.[37] Although this model is crude, it serves to evaluate the feasibility of performing the experiment. Certainly, more realistic calculations will be required in order to draw conclusions from the (e,e'p) data and such calculations are currently underway by several theoretical groups.

Single-arm background rates for (e,e') were calculated with the computer code QFSV and for (e,p), (e,π^+) and (e,π^-) with the electro-production code EPC.[38] The resulting single-arm cross sections were integrated over the appropriate spectrometer momentum acceptance and then multiplied by the spectrometer solid angle and luminosity in order to arrive at counting rates.

Quantity	Electron Arm	Proton Arm
momentum	±5%	±5%
θ_V	±65 mr	±65 mr
θ_H	±30 mr	±30 mr

Table 2 *Spectrometer acceptances used in the count rate estimates.*

For the L/T separation measurements, it is important to insure that comparable ranges of each physical variable are sampled for the forward and backward angle kinematics. This can be maintained to first order by applying cuts to the variables on which the response functions depend. In this analysis, a cut restricting the range of energy transfer, ω, for the forward angle run to match that for the backward angle was used. This also avoids sampling kinematics far from the quasielastic peak which would otherwise contribute due to the large spectrometer momentum bite at the forward electron angle. In addition, only comparable ranges of recoil momentum should be compared in performing the separation. This is accomplished by matching the angular phase space about the central $\vec{q}$ direction for the two kinematics. The ranges considered are given in Table 3. The range of p_r common to the forward and backward angle measurements is shown but no explicit cut was made on this variable. (For the forward angle measurements for all but the lowest Q^2 point, recoil momenta up to 0.25 GeV/c are sampled.) Here, $\Delta\theta_q^{H(V)}$ represents the cuts made on the horizontal (vertical) variation about the central $\vec{q}$ direction. The yield distributions versus recoil momentum as calculated by MCEEP are shown in Figure 9 for Kinematics

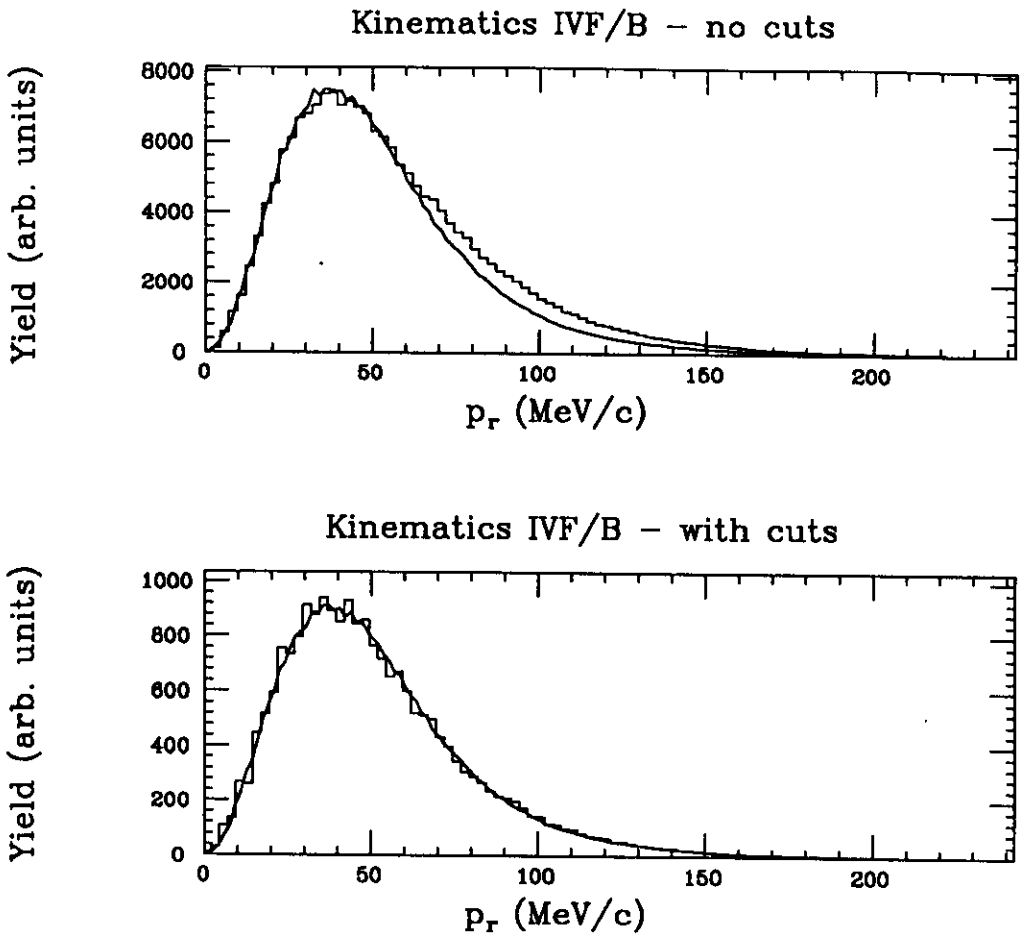

Figure 9. *Yield distributions versus p_r as calculated by MCEEP for Kinematics IV before and after cuts. The yields for the backward (forward) electron angle are shown as a solid curve (histogram).*

IV before and after cuts. The cuts result in a good matching of the distributions at both kinematics as is required for separation measurements.

The singles and coincidence counting rates and times are shown in Table 4A for the L/T separation measurements and in Tables 4B and 4C for the angular distribution measurements at the low Q^2 and high Q^2 respectively.

For the L/T separations, the (e,e′) singles and (e,e′p) coincidence rates as well as counting times reflect the cuts shown in Table 3. For Kinematics IF, the luminosity was lowered so that the maximum coincidence rate is 10^4. The uncut yields are significantly larger at the forward angles which may create some data processing bottlenecks at the lowest Q^2 points. However, the times involved in these measurements are minimal so that one could reduce the luminosity further with minimal impact. Running times were calculated assuming 1% statistics (average per 10 MeV/c bin in p_r for the range of p_r indicated in Table 3). The times at the forward angles have been increased beyond this to allow statistically precise measurements up to $p_r = 0.25$ GeV/c for the highest three Q^2 points. At this p_r the indicated times will provide 2%/3%/4% measurements per

Kinematics	ω range MeV	$\Delta\theta_q^V$ $\pm$ mr	$\Delta\theta_q^H$ $\pm$ mr	p_r range MeV/c
IF	113–141	36	20	0–40
IB				
IIF	417–453	22	20	0–60
IIB				
IIIF	1122–1168	16	10	0–80
IIIB				
IVF	1794–1852	18	10	0–100
IVB				

Table 3 *Acceptance matching cuts for the L/T separation measurements.*

Kin.	(e,e′) sec^{-1}	(e,π^-) sec^{-1}	(e,p) sec^{-1}	(e,π^+) sec^{-1}	trues sec^{-1}	accidentals sec^{-1}	Time hours
IF*	800000	4600	39000	11000	10000	2.23×10^{-1}	1
IB	30900	0	24800	0	3080	5.47×10^{-3}	1
IIF	109000	17000	43600	29500	883	1.28×10^{-2}	1
IIB	900	275	26600	0	349	6.47×10^{-5}	1
IIIF	791	15700	67000	32000	30.2	6.38×10^{-5}	10
IIIB	17.1	1460	43000	0	17.1	8.86×10^{-7}	2
IVF	40.5	14500	66000	9110	6.06	2.18×10^{-6}	20
IVB	3.06	3180	54000	0	3.34	1.35×10^{-7}	8
TOTAL							44
TOTAL incl. rad. corr.							56

Table 4A *Counting rates and times for the L/T separations. (* The luminosity for Kinematics IF was lowered to* 0.9×10^{38} $cm^{-2}sec^{-1}$.*)*

Kin	p_r range MeV/c	(e,p) sec^{-1}	(e,π^+) sec^{-1}	trues sec^{-1}	accid. sec^{-1}	S/N	Time (hours)
0A,B	0–100	43600	29500	3750	1.73×10^{-2}	2.17×10^{5}	1
0C		26600	0	384	8.71×10^{-5}	4.41×10^{6}	1
50A	0–100	111000	30400	2260	4.40×10^{-2}	5.14×10^{4}	1
50B		1420	30400	2140	5.63×10^{-4}	3.80×10^{6}	1
50C		6050	0	180	1.98×10^{-5}	9.09×10^{6}	1
100A	50–150	126000	31400	603	4.99×10^{-2}	1.21×10^{4}	1
100B		1400	27800	604	5.55×10^{-4}	1.09×10^{6}	1
100C		2440	0	33	7.99×10^{-6}	4.13×10^{6}	1
150A	100–200	138000	31800	151	5.47×10^{-2}	2.76×10^{3}	1
150B		1300	26500	170	5.16×10^{-4}	3.29×10^{5}	1
150C		2290	0	6.59	7.49×10^{-6}	8.80×10^{5}	1
200A	150–250	153000	32900	42	6.06×10^{-2}	693	1
200B		1200	25600	54.9	4.75×10^{-4}	1.16×10^{5}	1
200C		2260	0	1.65	7.40×10^{-6}	2.23×10^{5}	2
300A	250–350	180000	34100	4.33	7.13×10^{-2}	60.7	1
300B		1100	15100	7.88	4.37×10^{-4}	1.80×10^{4}	1
300C		2460	0	0.171	8.05×10^{-6}	2.12×10^{4}	16
400A	350–450	213000	35000	0.437	8.44×10^{-2}	5.18	8
400B		1100	4050	1.51	4.37×10^{-4}	3.50×10^{3}	2
400C		3150	0	0.0268	1.03×10^{-5}	2.60×10^{3}	104
500A	450–550	249000	36000	0.0951	9.87×10^{-2}	0.964	60
500B		1100	0	0.348	4.37×10^{-4}	800	8
500C*		4620	0	.00525	1.51×10^{-5}	348	132
TOTAL							347
TOTAL incl. rad. corr.							425

Table 4B *Counting rates and times for the angular distribution measurement at the low Q^2. Times assume 1% statistics summed over the indicated p_r range. The (e,e′) singles rate is 109000 sec^{-1} for Kinematics A and B and 900 sec^{-1} for Kinematics C. The (e,π^-) rate is 17000 sec^{-1} for Kinematics A and B and 275 sec^{-1} for Kinematics C. (* The statistics for Kinematics 500C were reduced to 2%.)*

Kin	p_r range MeV/c	(e,p) sec^{-1}	(e,π^+) sec^{-1}	trues sec^{-1}	accid. sec^{-1}	S/N	Time (hours)
0D,E	0–50	67000	32000	71.0	6.63×10^{-5}	1.07×10^{6}	1
100D	50–150	159000	37000	28.0	1.57×10^{-4}	1.78×10^{5}	1
100E		450	12000	29.4	4.45×10^{-7}	6.61×10^{7}	1
200D	150–250	166000	39000	1.38	1.64×10^{-4}	8.42×10^{3}	2
200E		424	0	1.92	4.19×10^{-7}	4.58×10^{6}	2
300D	250–350	175000	39000	0.128	1.73×10^{-4}	740	5
300E		395	0	0.249	3.91×10^{-7}	6.37×10^{5}	3
TOTAL							15
TOTAL incl. rad. corr.							20

Table 4C *Counting rates and times for the high Q^2 angular distribution measurement. Times assume 1% statistics summed over the indicated p_r range except for the 300 MeV/c recoil momentum points where 2% statistics are assumed. The (e,e′) singles rate is 791 sec^{-1}. The (e,π^-) rate is 15700 sec^{-1}.*

10/10/20 MeV/c p_r bin for Kinematics IIF/IIIF/IVF. Since the cross sections do not include radiative effects, we have estimated radiative correction factors of 30% and 20% for the forward and backward angle measurements respectively and have increased our total time estimate accordingly. It is seen that adequate statistics can be acquired in a reasonable amount of time even at the highest momentum transfer.

For the low Q^2 angular distribution measurement the counting times are based on 1% statistics integrated over the indicated p_r range except for Kinematics 500C where the statistics are 2%. In order to restrict the electron kinematics to the quasielastic peak and for comparison to the L/T separation measurements, coincidence rates were calculated with a cut on ω: $0.417 \leq \omega \leq 0.453$ GeV, and on the angular range of $\vec{q}$ as in Kinematics II.

Finally, for the high Q^2 angular distribution measurement the counting times are based on 1% statistics integrated over the indicated p_r range except for the 300 MeV/c recoil momentum points where 2% statistics are assumed. The rates also include a cut on ω: $1.122 \leq \omega \leq 1.168$ GeV in order to restrict the kinematics to the quasielastic peak. However, there are no cuts on the angular range of $\vec{q}$ as there is no backward angle measurement and hence no matching requirement.

For all measurements, the accidentals rates assume a coincidence resolving time of 2 ns (full width at base). (The timing resolution is expected to be better than 2 ns but this

will not improve the signal-to-noise ratio because of the 2 ns substructure of the beam.) In addition the accidentals rates assume target-vertex cuts and missing mass cuts. Given the spectrometers' transverse position resolution of ± 1 mm, the resolution along the target length is roughly 1 cm for the worst case with the spectrometer at 12.5°. Vertex consistency checks between the two spectrometers can thus reduce the accidental background by about a factor of 10 for a 10 cm long target. In addition, assuming a missing mass resolution of 1 MeV, the total enhancement in signal-to-noise due to missing mass and vertex cuts is at least 280/740/1660/2450 for Kinematics I/II/III/IV and at least 550 (1600) for each of the angular distribution measurements at the low (high) Q^2. The signal-to-noise ratio is about 1:1 for the worst case (Kinematics 500A) after inclusion of these cuts. (The signal-to-noise ratios for the L/T separation kinematics are very large and therefore not tabulated.) The highest recoil momentum measurements would be severely signal-to-noise limited if it were not for the excellent traceback properties of the Hall A spectrometer pair.

The accidentals rates and signal-to-noise exclude contributions from $\pi^{\pm}$ and therefore assume good particle identification in both arms. To achieve the required rejection ratios for pions we plan to use both shower and Čerenkov counters in the focal plane. From Tables 4A, 4B and 4C, the instantaneous counting rates are not expected to be a problem from the point of view of π rejection. The π^-/e ratio is 1000:1 for the worst case (L/T Kinematics IVB). However, since the pion singles yields will be distributed with respect to time-of-flight, missing mass and target vertex position the pion contamination after all cuts should be less than 1:1. Thus only modest rejection ratios are required of the particle ID detectors. In general, correlated backgrounds from (e,e$'\pi^+$) and $(\gamma, \pi^- \mathrm{p})$ need to be considered as well. (Uncorrelated events can be eliminated by background subtraction but event-by-event recognition will be desirable to enhance the signal-to-noise ratio.) For the case at hand where the kinematics are quasielastic, $(\gamma, \pi^- \mathrm{p})$ requires a photon energy near the endpoint. Thus, we do not expect this process to dominate the correlated yield. Furthermore, the (e,e$'\pi^+$) process is not allowed kinematically for these experiments. Hence, for now these correlated backgrounds are neglected although it would be desirable to have actual estimates in the future.

4. Analysis of Systematic Uncertainties

Uncertainty in the reaction kinematics is expected to be the dominant source of systematic error due to the rapid variation of the (e,e$'$p) cross section. Further, because of the relatively large spectrometer acceptances, the cross section varies appreciably within the coincidence acceptance volume. Therefore the data cannot be averaged over the entire acceptance but must be divided into a set of bins where the bin for a given event is defined by combinations of the coordinates measured in the focal planes of each of the two spectrometers. Each bin's centroid must be located precisely in order to allow quantitative comparisons with theoretical models. In addition, because of the relatively small size of the longitudinal response function (especially at large Q^2), its extraction requires that errors in the cross sections be kept to a minimum. For L/T separation experiments, due to the differential sensitivities of the cross sections at each kinematics, absolute knowledge of the

particle angles and momenta is required.[39] To estimate uncertainties in the cross sections arising from inaccuracies in determination of the reaction kinematics, a sensitivity study was performed using MCEEP.

The results of the sensitivity study for the low Q^2 angular distribution measurements are shown in Figures 10–12 for the A, B and C kinematics respectively. These figures show the relative error in the cross sections arising from uncertainty in each of the kinematical quantities. Here e (e') is the incident (scattered) electron energy and θ_b, θ_e and θ_p are the in-plane angles of the beam, scattered electron and proton respectively. (The calculations are performed for a fixed missing mass of 2.2 MeV so that the proton momentum is determined from the other five variables. In principle a redundant measurement of the proton momentum can help to reduce the total systematic error although in practice one must also account for radiative effects which result in a missing energy tail.) In order to avoid inaccuracies in the calculation of the errors, MCEEP was run with measurement uncertainties ten times larger than those we hope to ultimately achieve in Hall A. Figure 13 shows the total uncertainty formed by adding all errors in quadrature for the "ultimate" measurement uncertainties given in Table 5. (These uncertainties are 10 times smaller than those in Figures 10–12.) In each of the figures three curves are displayed. The dotted curve corresponds to a point acceptance, the dashed curve is for the full spectrometer acceptance but with the cuts on ω and the angles of $\vec{q}$ described above and the solid curve is with the ω cut only. The errors tend to be maximum near $p_r = 0.05$ GeV/c where the deuteron momentum distribution is most rapidly varying. However, it is evident that averaging over the experimental acceptance tends to minimize the uncertainties. The total uncertainty for Kinematics A/B/C for the full set of cuts peaks at roughly 2.0%/1.6%/0.6% and is comparable to the statistical error for these measurements (within a factor of two). The backward angle kinematics is least sensitive allowing a fairly accurate determination of the transverse response. Further, it was demonstrated earlier that in the context of the Arenhövel and Tjon calculations an interesting measurement results even with uncertainties three times larger than the "ultimate" ones.

Variable	Uncertainty
e	10^{-4}
e'	10^{-4}
θ_b	0.1 mr
θ_e	0.1 mr
θ_p	0.1 mr

Table 5 *Kinematical uncertainties. These are the ultimate goals of the Hall A apparatus. An analysis was also carried out assuming errors three times larger and is described in the text.*

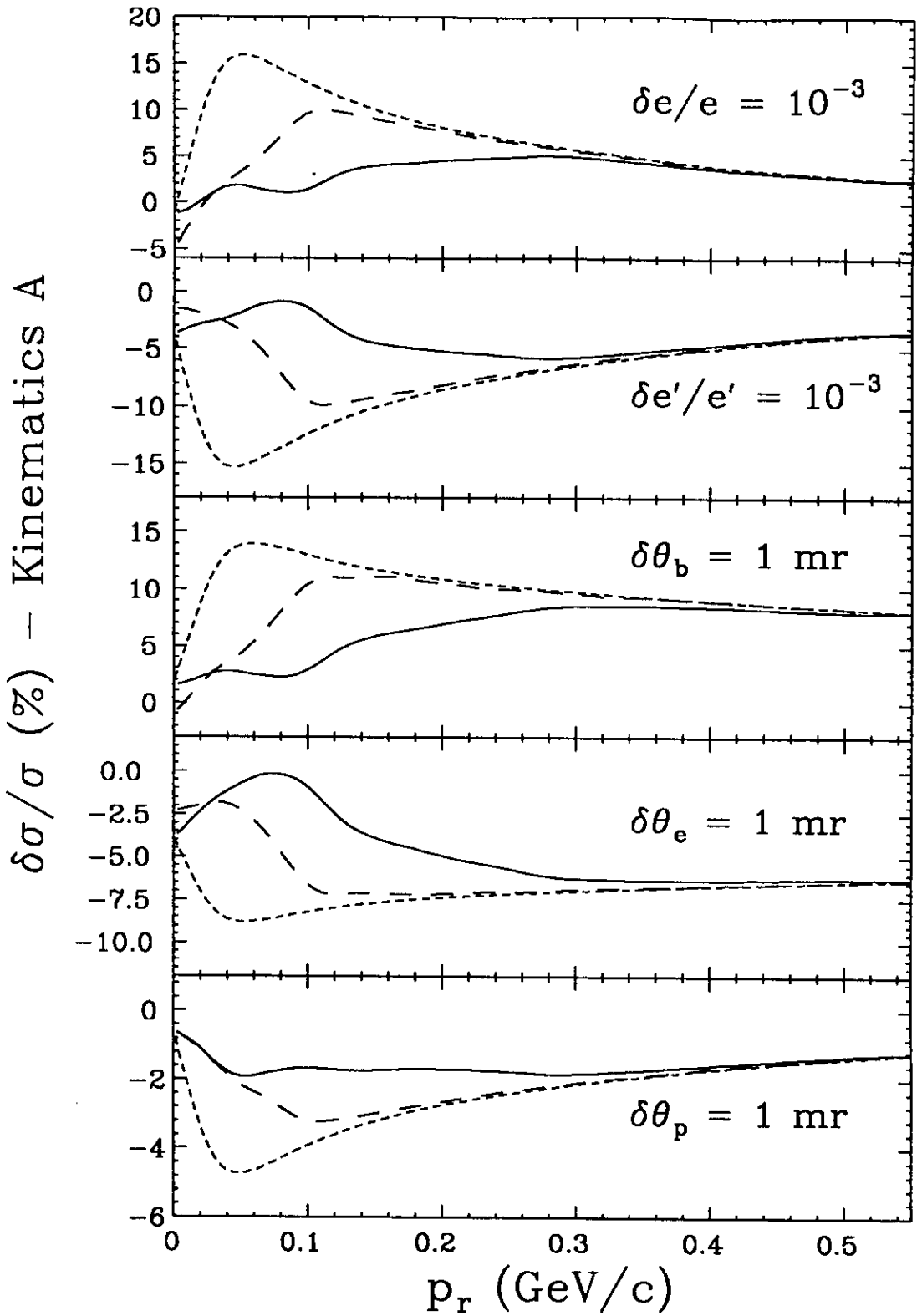

Figure 10. *Relative error in the d(e,e'p)n cross section for the angular distribution study for Kinematics A given the kinematical uncertainties shown. The kinematical uncertainties used here are artificially large so as to minimise inaccuracies in the evaluation of the errors. The curves are described in the text.*

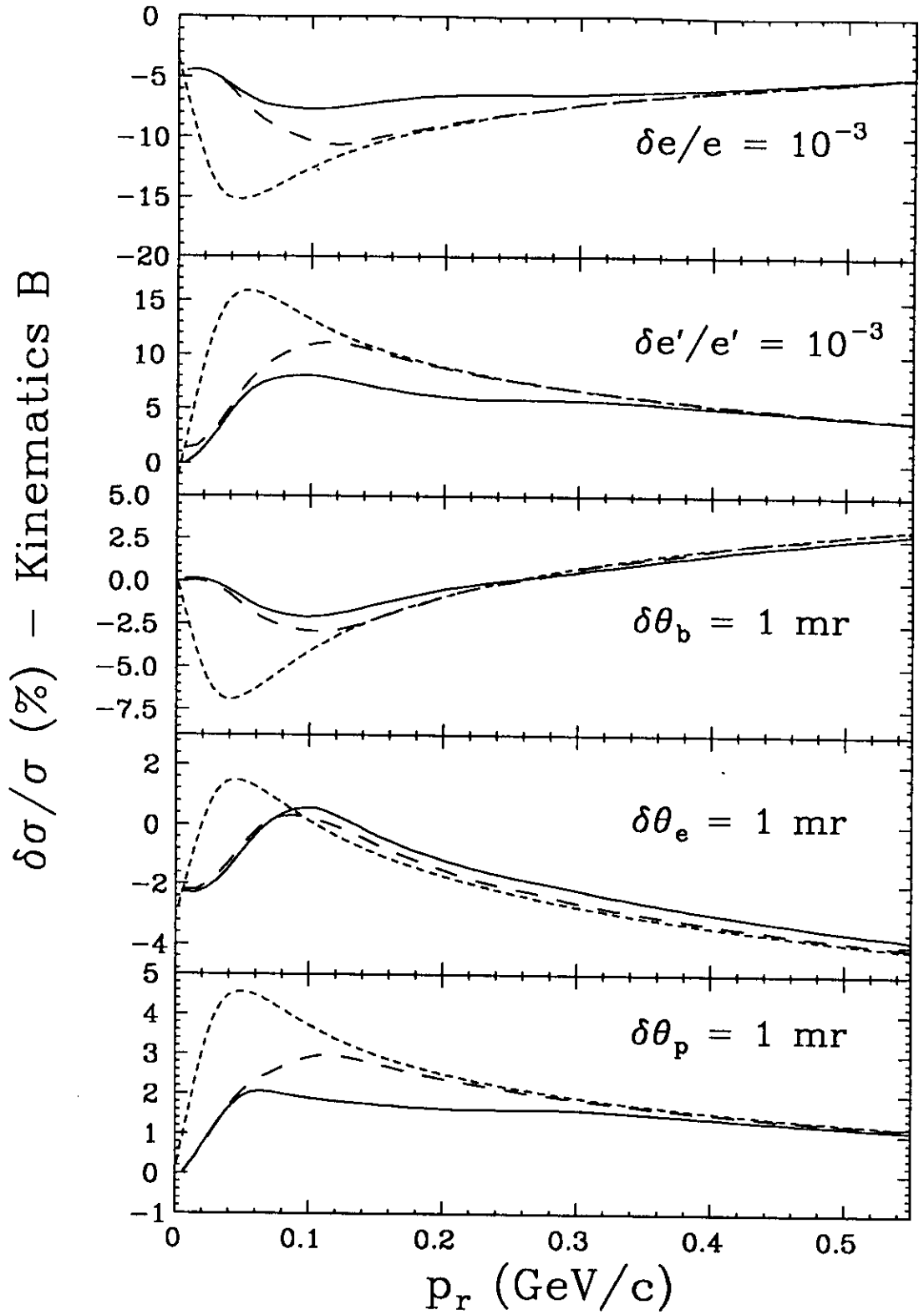

Figure 11. *Same as figure 10, but for Kinematics B.*

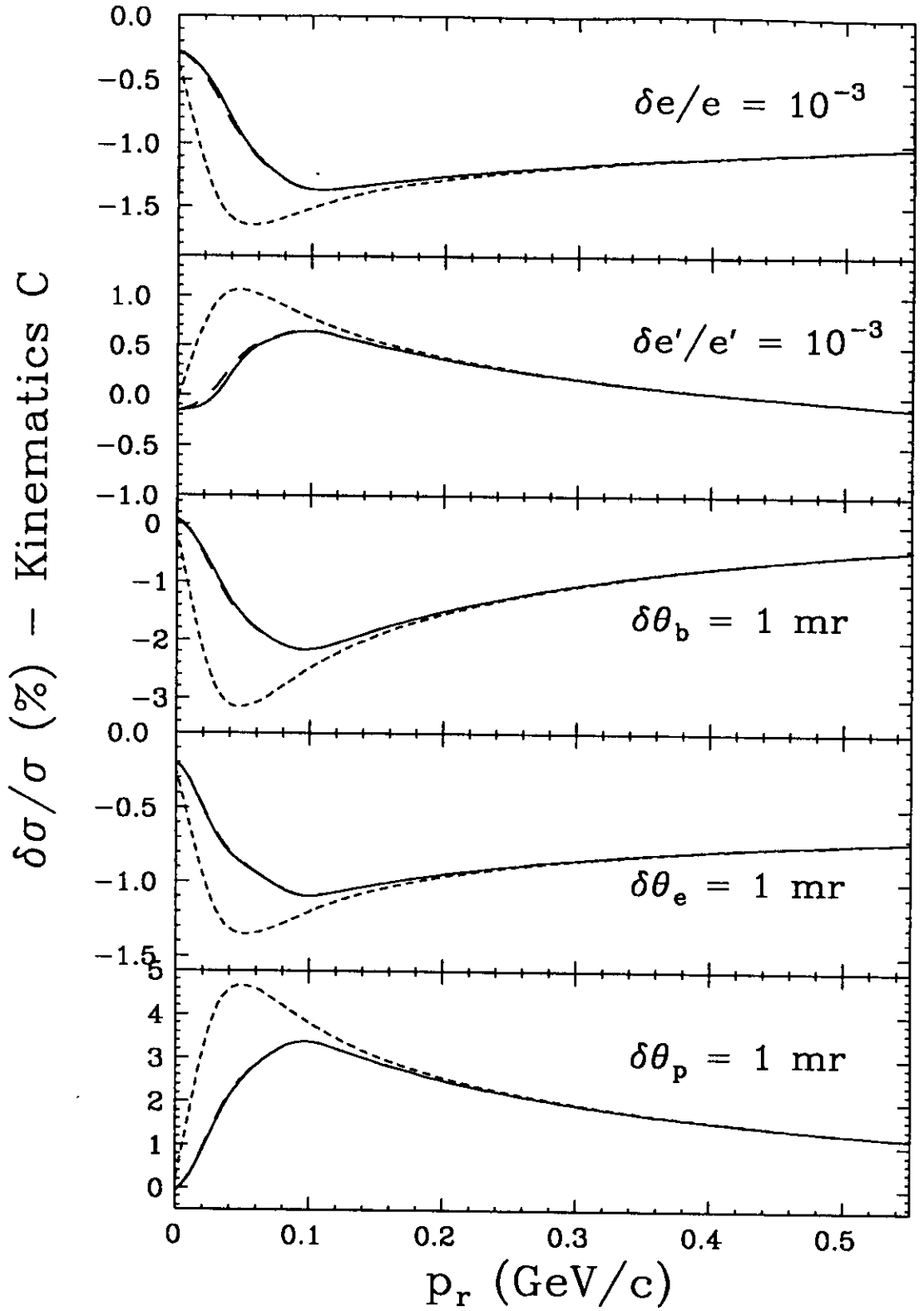

Figure 12. *Same as figure 11, but for Kinematics C.*

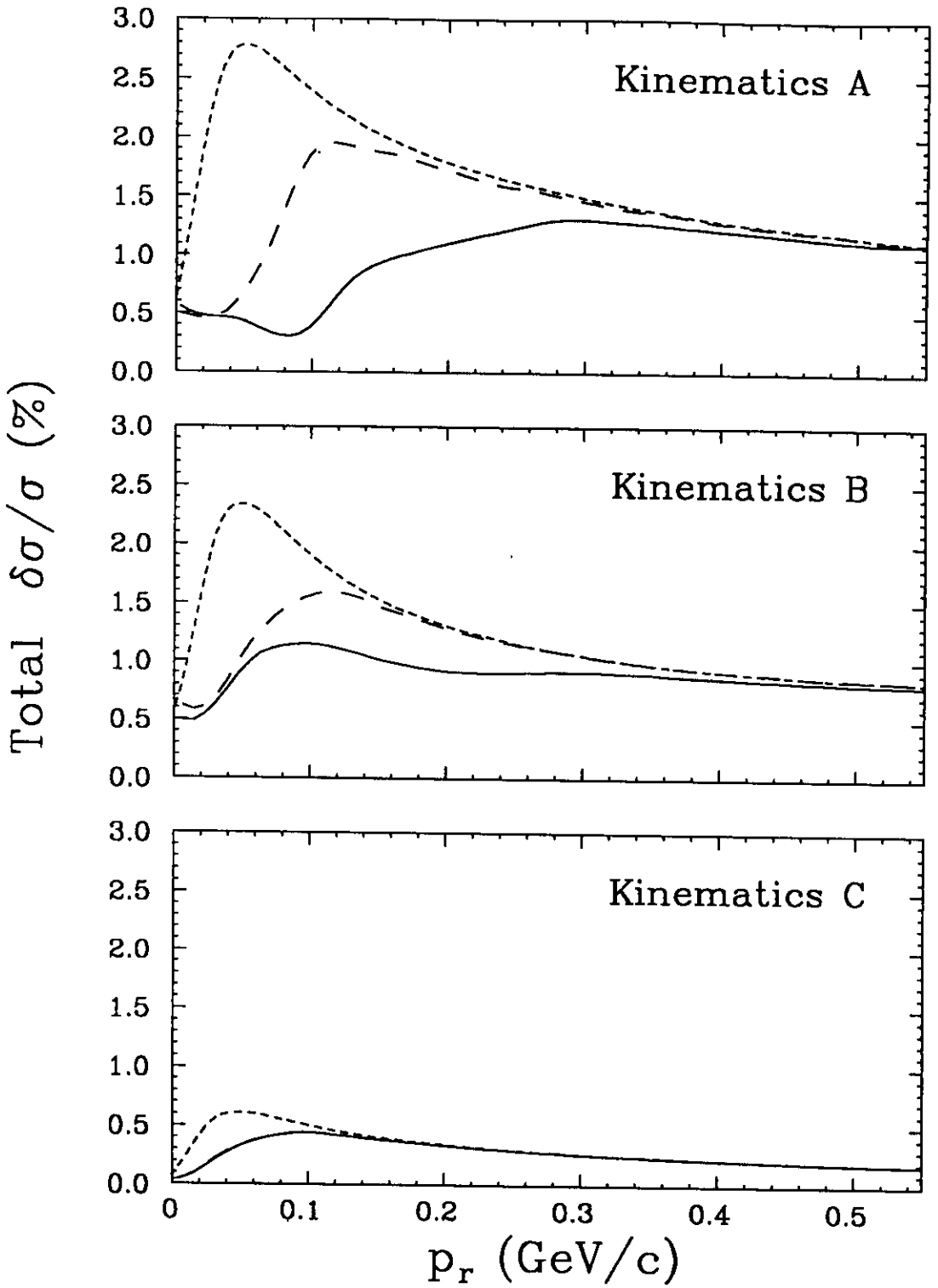

Figure 13. *The total error obtained from the previous three figures and the "ultimate" measurement uncertainties given in Table 5.*

As is evident from the previous figures, at quasielastic kinematics ($p_r = 0$) kinematical sensitivities with respect to a global shift are minimized since the momentum distribution is averaged over symmetrically. This has important consequences for the L/T separation measurements. The errors for the L/T measurements have been calculated for point acceptances[40] and are displayed in Table 6. The total errors assume the ultimate measurement uncertainties. The errors are quite small although they will be somewhat larger for a finite acceptance about $p_r = 0$ as indicated by the previous study for the angular distribution measurements. In addition, correlated errors in the spectrometer field map across the acceptance will partially destroy this symmetric averaging and result in larger errors. Nonetheless, by restricting oneself to the region around $p_r = 0$ one can hope to perform accurate separations of the R_L and R_T response functions in d(e,e'p)n.

Kin.	e %/MeV	θ_b %/mr	e' %/MeV	θ_e %/mr	θ_p %/mr	Total Error %
IF	1.7	0.069	0.37	0.39	0.097	0.28
IB	1.6	0.0047	0.27	0.025	0.082	0.063
IIF	0.53	0.64	0.17	0.19	0.13	0.23
IIB	0.54	0.060	0.064	0.0070	0.059	0.044
IIIF	0.28	0.54	0.068	0.20	0.069	0.13
IIIB	0.29	0.013	0.013	0.0031	0.018	0.047
IVF	0.22	0.42	0.013	0.22	0.039	0.10
IVB	0.21	0.050	0.057	0.025	0.014	0.050

Table 6 *Systematic uncertainties in the cross sections for the L/T separation measurements assuming "point" acceptances.*

Determination of the longitudinal response function becomes increasingly difficult with increasing $\vec{q}$ due to its small relaive size. In Table 7 the uncertainties in R_L and R_T are given assuming statistical uncertainties of 1% in the cross sections as well as for the systematic uncertainties of Table 6. These errors also assume the values of R_L/R_T given by our model calculation at the central kinematics. One percent measurements of the cross sections (total uncertainty) would provide a 22% measurement of R_L at the highest $\vec{q}$ studied. Although the kinematical domain accessible to CEBAF is somewhat larger, $\sim$ 3 GeV/c appears to be the practical limit for these separation measurements.

Other sources of error which have been ignored in this analysis include uncertainties in target thickness and beam current. Since overall normalization errors do not get magnified in extracting response functions from cross sections, the absolute luminosity need not be

$\vec{q}$ GeV/c	R_L/R_T	$\delta R_L/R_L$ (%) statistical	$\delta R_T/R_T$ (%) statistical	$\delta R_L/R_L$ (%) systematic	$\delta R_T/R_T$ (%) systematic
0.5	1.000	2.6	2.5	0.63	0.37
1.0	0.309	4.5	1.3	0.84	0.08
1.9	0.139	12	1.2	1.2	0.06
2.6	0.116	22	1.3	1.8	0.07

Table 7 *Systematic errors in the response functions.*

known as accurately as the relative luminosity among the various measurements in the separation experiment. The luminosity should be known absolutely at the few percent level and relatively at the fraction of a percent level. Samples of the single-arm cross sections will be used as an internal check on luminosity variations at a given kinematical setting.

5. Experimental Equipment

The high resolution capabilities of the Hall A spectrometers are essential in carrying out this experiment. It has been demonstrated that the resolution is needed to control the systematic errors arising from uncertainties in the reaction kinematics. In addition, in order to maintain a favorable signal-to-noise ratio at high recoil momenta, good missing mass and vertex resolution are required. The dynamic range of this experiment requires spectrometers with a momentum range of $\sim$ 0.3 GeV/c to 4 GeV/c with a premium on reaching small angles. Details of the spectrometers and instrumentation can be found in the Hall A Conceptual Design Report.[41]

High power target cells meeting the requirements for these measurements are being developed by members of the Hall A collaboration. Although it would be advantageous to have two cells, one for deuterium and one for the hydrogen normalizations, it appears that the initial complement of equipment in Hall A will provide for only one. Therefore, overhead for emptying and filling the cell has been estimated and added to the total beam time request. Because of the need for precision we plan on restricting the maximum beam current to 50 μA (for a maximum luminosity of 1.5×10^{38} cm^{-2}sec^{-1} for 10 cm of liquid deuterium) in order to avoid large target density fluctuations. The power dissipation in the target for this beam current is 290 Watts (this assumes the standard 15 cm cell; the count rates assume that only 10 cm can be viewed by the spectrometers). In addition to the cryogenic targets, we will need to have CH_2 and ^{12}C targets in the ladder for additional normalization checks. Also, a BeO screen will be required for alignment checks.

6. Beam Time Summary

The beam time needed to complete these measurements is shown in Table 8. Table 9 shows the beam time required for each beam energy. Although an operating scenario has not yet been worked out for CEBAF we have estimated a one hour overhead associated with each angle/field change. Without a dual-cell cryotarget, 12 hours have been allotted for each cryogenic hydrogen–deuterium target change. In addition, based on previous experience about 48 hours will be required for calibration and normalization measurements. With a luminosity of 81 μA-g/cm^2 the total beam time is 700 hours. We expect that the program on d(e,e′p)n will form the basis of a number of Ph.D. theses with 2 to 4 theses resulting from this initial study.

Measurement	time (hours)
R_L/R_T	56
Angular Distribution (low Q^2)	425
Angular Distribution (high Q^2)	20
Norm./Calib.	48
Field/Angle changes	55
Cryo-Target Changes	96
TOTAL	700

Table 8 *Beam time summary.*

Beam Energy (GeV)	time (hours)
0.4	2
0.8	340
1.6	4
2.4	10
4.0	193
Overhead	151
TOTAL	700

Table 9 *Beam time required for each energy.*

7. Acknowledgements

I would like to thank J.D. Walecka, R. Ent, M. Epstein, J.M. Finn, J. Gomez, J. Mitchell and R. Schiavilla for their contributions to this proposal. I also thank J. Tjon for providing theoretical calculations and for useful discussions.

Appendix: Sensitivity to Off-shell Effects

In the absense of final state interactions the half-off-mass-shell nucleon transition matrix element from a state of momentum k to momentum k' can be parametrized as a function of two invariant amplitudes:

$$(j_\mu j_\nu)^N = W_2(Q^2,\chi)\tilde{k}_\mu\tilde{k}_\nu + W_1(Q^2,\chi)\left(\delta_{\mu\nu} - \frac{q_\mu q_\nu}{q^2}\right)$$

where $\tilde{k}_\mu = [k_\mu - (k \cdot q/q^2)q_\mu]$ and $\chi = (m^{*2} - m^2)/q^2$ with $k^2 = m^{*2}$ and $k'^2 = m^2$. The dimensionless quantity χ characterizes the off-mass-shell kinematics. Ignoring the small binding energy term, at the top of the quasielastic peak $\chi = 0$. χ grows with recoil momentum and approximately as $\frac{M_A}{M_{A-1}}\frac{k^2}{q^2}$. Therefore, the kinematical effects of the off-mass-shell initial state, although expected to be small, grows with k^2. Paradoxically, the kinematical constant is largest for d(e,e'p) because of the small recoil mass. It can be studied by measurements at different q^2 in the context of a reaction model.

To illustrate the sensitivity of the proposed experiment to the form of the electromagnetic current operator, the half-off-shell *ep* cross sections arising from various choices are shown in Figure 14 relative to the de Forest "CC1" prescription.[20] The models deviate most strongly at low Q^2 and for lighter systems. The proposed experiment will probe recoil momenta up to 0.25 GeV/c as a function of Q^2 with maximum statistical errors of 2%/3%/4% per 10/10/20 MeV/c bin in p_r for $Q^2 = 0.811/2.139/3.408$ GeV^2/c^2. In addition to these kinematical effects there can be dynamical effects which manifest themselves in terms of modified form factors.

Of course, one must be cautious attributing any apparent "deviations" to off-shell effects in the light of our present lack of understanding of details of the model for the deuteron. To further this understanding is, in fact, the goal of this experiment.

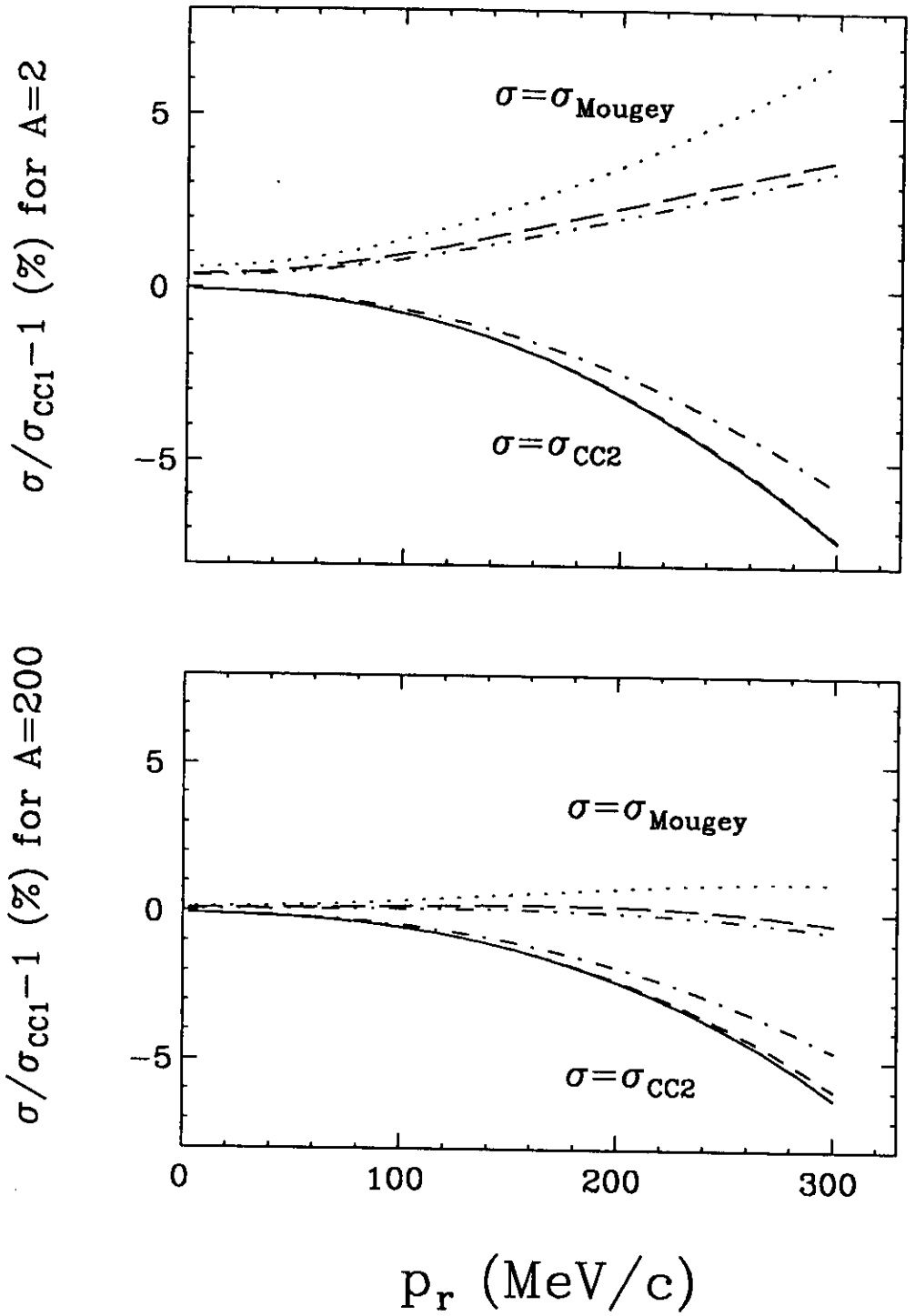

Figure 14. *Deviations of off-shell ep cross sections for various choices of current operator relative to the de Forest "CC1" prescription. The top panel is for A=2 (deuteron) and the bottom for A=200. Each of the three curves for a given model corresponds to one of the three highest proposed Q^2 points. The outer curves are for $Q^2 = 0.811$ GeV^2/c^2, the middle curves are for $Q^2 = 2.139$ GeV^2/c^2 and the inner curves are for $Q^2 = 3.408$ GeV^2/c^2. The models deviate most strongly for the lower Q^2 points and for A=2 compared to A=200.*

References

[1] K.B. Unser, *Design and Preliminary Tests of a Beam Monitor for LEP*, CERN/LEP-BI/89-07 (1989); K. Unser, IEEE Trans Nucl. Sci. **28**, 2344 (1981); K. Unser, IEEE Trans. Nucl. Sci. **16**, 934 (1969).

[2] P.E. Ulmer, I Karabekov, A. Saha, P. Bertin and P. Vernin, *Absolute Beam Energy Determination at CEBAF*, CEBAF Technical Note 94-001 (1994).

[3] P. Welch and R. Ent, *Energy Measurement of Electron Beams by Compton Scattering*, unpublished (1994).

[4] S. Auffret *et al.*, Phys. Rev. Lett. **55**, 1362 (1985); R.G. Arnold *et al.*, Phys. Rev. C**42**, R1 (1990).

[5] I. The *et al.*, Phys. Rev. Lett. **67**, 173 (1991); R. Gilman *et al.*, Phys. Rev. Lett. **65**, 1733 (1990); M.E. Schulze *et al.*, Phys. Rev. Lett. **52**, 597 (1984).

[6] C. Marchand *et al.*, Phys. Rev. Lett. **60**, 1703 (1988).

[7] K.F. von Reden *et al.*, Phys. Rev. **C41**, 1084 (1990); R. Schiavilla *et al.*, Phys. Rev. **C40**, 1484 (1989); G. Orlandini and M. Traini, Phys. Rev. **C31**, 280 (1985); Z.E. Meziani *et al.*, Phys. Rev. Lett. **52**, 2130 (1984); P. Barreau *et al.*, Nuovo Cim. **76A**, 361 (1983).

[8] W. Fabian and H. Arenhövel, Nucl. Phys. **A314**, 253 (1979).

[9] M. van der Schaar *et al.*, Phys. Rev. Lett. **68**, 776 (1992).

[10] E. Hummel and J.A. Tjon, Phys. Rev. C**49**, 21 (1994).

[11] S. Galster *et al.*, Nucl. Phys. **B32**, 221 (1971).

[12] A. Lung *et al.*, Phys. Rev. Lett. **70**, 718 (1993).

[13] R.G. Arnold, C.E. Carlson and F. Gross, Phys. Rev. C **23**, 363 (1981); H. Arenhövel, W. Leidemann and E.L. Tomusiak, Z. Phys. A **331**, 123 (1988).

[14] H. Arenhövel, Phys. Lett. **B199**, 13 (1987) and private communication; A.Yu. Korchin, Yu.P. Mel'nik and A.V. Shebeko, Sov. J. Nucl. Phys. **48**, 243 (1988); M.P. Rekalo, G.I. Gakh and A.P. Rekalo, J. Phys. G. **15**, 1223 (1989).

[15] Bates Experiment 85-05, R. Madey and S. Kowalski cospokesmen, to be published.

[16] CEBAF Proposal 89-005, *The Electric Form Factor of the Neutron from the* $d(\vec{e},e'\vec{n})p$ *Reaction*, R. Madey spokesman.

[17] M. Bernheim *et al.*, Nucl. Phys. **A365**, 349 (1981).

[18] M. van der Schaar, Ph.D. thesis, Rijksuniversiteit te Utrecht (1991).

[19] Bates Proposal 88-21, *Polarization Transfer Measurements in the* $D(\vec{e},e'\vec{p})n$ *Reaction*, J.M. Finn, R.W. Lourie, C. Perdrisat and P.E. Ulmer cospokesmen; CEBAF Proposal 89-028, *Polarization Transfer Measurements in the* $D(\vec{e},e'\vec{p})n$ *Reaction*, J.M. Finn and P.E. Ulmer cospokesmen.

[20] T. de Forest, Jr., Nucl. Phys. **A392**, 232 (1983); J. Mougey *et al.*, Nucl. Phys. **A262**, 461, (1976).

[21] M. Gourdin, Nuovo Cim. **21**, 1094 (1961).

[22] A. Picklesimer and J.W. Van Orden, Phys. Rev. **C35**, 266 (1987).

[23] V. Punjabi *et al.*, Phys. Rev. **C38**, 2728 (1988).

[24] C.F. Perdrisat *et al.*, Phys. Rev. **187**, 1201 (1969); T.R. Witten *et al.*, Nucl. Phys. **A254**, 269 (1975); R.D. Felder *et al.*, Nucl. Phys. **A264**, 397 (1976).

[25] M.B. Epstein *et al.*, Phys. Rev. **C42**, 510 (1990).

[26] M. Lacombe *et al.*, Phys. Lett. **101B**, 139 (1981).

[27] Franz Gross, J.W. Van Orden and Karl Holinde, Phys. Rev. **C45**, 2094 (1992).

[28] F. Krautschneider, Ph.D. Thesis, Bonn University, BONN-IR-76-37 (1976); L. Hulthen and M. Sagawara, Handb. d. Phys. Bd. 39, S.1.

[29] S. Turck-Chieze *et al.*, Phys. Lett. **142B**, 145 (1984).

[30] T. Tamae *et al.*, Phys. Rev. Lett. **59**, 2919 (1987).

[31] M. van der Schaar *et al.*, Phys. Rev. Lett. **66**, 2855 (1991).

[32] SLAC NE-18 experiment; R. Ent, private communication.

[33] H. Arenhövel, private communication.

[34] A. Yu. Korchin, Yr. P. Mel'nik and A.V. Shebeko, Yad. Fiz. **48**, 387 (1988); M.P. Rekalo, G.I. Gakh and A.P. Rekalo, J. Phys. G. **15**, 1223 (1989); J.M. Laget, private communication.

[35] J.W. Van Orden and F. Gross, private communication.

[36] J. Tjon, private communication.

[37] P.E. Ulmer, *MCEEP: Monte Carlo for Electro-Nuclear Coincidence Experiments*, CEBAF Technical Note 91-101 (1991).

[38] J.W. Lightbody and J.S. O'Connell, Computers in Physics, May/June 1988, p. 57.

[39] P.E. Ulmer *et al.*, *Physics Requirements on the Determination and Stability of the Parameters of the Beam*, CEBAF Technical Note 90-255 (1990).

[40] P.E. Ulmer, Computer Program SIGEEP (1987).

[41] *Conceptual Design Report, Basic Experimental Equipment*, CEBAF, Newport News, VA 23606, April 13, 1990.